

# Infrared and X-ray Photoelectron Spectroscopic Studies of the Reactions of Hydrogen-Terminated Crystalline Si(111) and Si(100) Surfaces with Br<sub>2</sub>, I<sub>2</sub>, and Ferrocenium in Alcohol Solvents

Joel A. Haber<sup>†</sup> and Nathan S. Lewis\*

Division of Chemistry and Chemical Engineering, California Institute of Technology, 127-72 Noyes Laboratory, Pasadena, California 91125

Received: January 24, 2001; In Final Form: January 3, 2002

The reaction chemistry of H-terminated crystalline Si(111) and Si(100) surfaces in CH<sub>3</sub>OH, CD<sub>3</sub>OD, CF<sub>3</sub>(CH<sub>2</sub>)<sub>3</sub>-OH, C<sub>4</sub>H<sub>9</sub>OH, and C<sub>4</sub>D<sub>9</sub>OD solutions containing ferrocenium (Fc<sup>+</sup>)-BF<sub>4</sub>, I<sub>2</sub>, or Br<sub>2</sub> was monitored using X-ray photoelectron (XP) spectroscopy and infrared (IR) spectroscopy. Addition of the one-electron oxidant Fc<sup>+</sup>, or addition of the oxidizing species I<sub>2</sub> or Br<sub>2</sub>, produced diagnostic changes in the IR spectra that clearly indicated formation of surficial Si-OR groups. XPS data confirmed the conclusions of the IR studies. Under our reaction conditions, no detectable reaction occurred without the presence of the oxidant. The data are consistent with oxidative activation of the surficial Si-H bonds toward nucleophilic attack by the alcohols. The reaction chemistry was generally similar on (111)- and (100)-oriented Si surfaces, although some differences were observed in the ratio of reaction products on the two different surface orientations. Alkoxyated surfaces were also prepared by a two-step process in which the surface was first chlorinated and then reacted with LiOCH<sub>3</sub>, LiOCD<sub>3</sub>, or LiO(CH<sub>2</sub>)<sub>3</sub>CF<sub>3</sub>. The data indicate that formation of silicon-halogen bonding alone is not sufficient to provide a robust correlation between the electronic and chemical properties of such crystalline Si surfaces and that formation of silicon-alkoxyl bonds is a common motif for surfaces often used in electronic and electrochemical studies of Si.

## I. Introduction

Several wet chemical approaches have recently been developed to functionalize nonoxidized, H-terminated Si surfaces. Such methods include chlorination and bromination,<sup>1–5</sup> alkylation by reacting the halogenated surface with Grignard reagents or with lithium alkyls,<sup>1,3,4</sup> alkylation using addition of olefins to the H-terminated surface induced by UV irradiation,<sup>2–4,6–9</sup> free-radical initiation,<sup>10,11</sup> thermal activation,<sup>11–13</sup> or hydrosilylation,<sup>6,14</sup> direct reaction of the H-terminated surface with bromine-containing Grignard reagents,<sup>6,15,16</sup> and functionalization using anodic<sup>17,18</sup> or cathodic<sup>19,20</sup> electrochemical processes. In addition to surface attachment via formation of Si-C bonds, organic reagents have been bound to the surface via Si-N, Si-S, or Si-O bonds through reaction of the chlorinated Si surface with amines,<sup>21,22</sup> thiols,<sup>5</sup> or alcohols,<sup>23</sup> respectively. Surface functionalization of H-terminated, single-crystal Si via Si-O bonds has also been reported by photoelectrochemical reaction with carboxylic acids,<sup>24</sup> photochemical reaction with aldehydes,<sup>8</sup> thermal reaction with aldehydes,<sup>25</sup> and thermal reactions with alcohols with<sup>26</sup> and without<sup>16,25,27–30</sup> the presence of dissolved oxidants. Porous Si surfaces have been extensively modified using both solution-phase and gas-phase reactions.<sup>31–34</sup> Si surfaces prepared in ultrahigh vacuum (UHV) have been functionalized<sup>35</sup> through the use of Diels-Alder reactions<sup>36,37</sup> and through reactions of an olefin with a surface-propagated radical chain reaction on the H-terminated 2 × 1 Si(100) surface.<sup>38</sup> Motivation for modification of Si surfaces includes enhancing stability against oxidation or corrosion reac-

tions,<sup>18,31–34,39,40</sup> passivation of electrical defect sites on the Si surface,<sup>41–46</sup> formation of ultrathin barrier layers for MOSFET-like devices,<sup>11,18,47</sup> and control over nucleation and growth of metals during electrodeposition or physical deposition processes involved in the formation of silicon/metal contacts.

It is well-documented that crystalline (111)-oriented Si surfaces can be prepared chemically, through etching in NH<sub>4</sub>F(aq), to have a nearly perfect termination with hydrogen, with the resulting Si-H bonds oriented perpendicular to the (111) surface plane.<sup>48–51</sup> The structure of the 48% HF(aq)-etched (100) Si surface is less-well defined, although this face is also believed to be predominantly H-terminated.<sup>48</sup> Oxidative functionalization of these surfaces is of interest because several groups have reported that the electrical recombination velocity of Si(100) and Si(111) surfaces is very low during contact with alcoholic solutions of halogens.<sup>41–46</sup> For example, effective surface recombination velocities, *S*, of <10 cm s<sup>-1</sup> were observed for p-type Si(100) and n-type Si(111) while in contact with 0.08 M I<sub>2</sub> in ethanol.<sup>43</sup> Similarly, *S* values of ≤0.75 cm s<sup>-1</sup> have been reported for Si(100) surfaces in contact with 0.005 M I<sub>2</sub> in CH<sub>3</sub>OH.<sup>44</sup> Immersion of H-terminated (111)-oriented Si into CH<sub>3</sub>OH-Br<sub>2</sub> solutions produces air-stable Si-Br bonds that have been detected by X-ray standing wave (XSW) methods, in which Br atoms form <24% of a monolayer on the Si(111) surface with a coherent fraction of Br occupying atop sites with a Si-Br bond length of 2.17 ± 0.04 Å.<sup>52–56</sup> A similar coherent fraction of Br was found by XSW methods after deposition of Br onto UHV-prepared (non-H-terminated) Si(111) surfaces.<sup>57,58</sup> X-ray standing wave measurements have apparently not been performed on H-terminated Si(111) surfaces that have been exposed to CH<sub>3</sub>OH-I<sub>2</sub> solutions; however, XSW measurements

\* To whom correspondence should be addressed.

<sup>†</sup> Present Address: Department of Chemistry, University of Alberta, Edmonton, Alberta T6G 2G2, Canada.

on UHV-prepared (non-H-terminated) Si(111) surfaces after deposition of 1.2 monolayers of I from a AgI electrolytic cell have indicated that a  $1 \times 1$  surface is obtained with 18% of a monolayer of I on atop sites,<sup>59</sup> similar to the surface obtained by  $\text{CH}_3\text{OH}-\text{Br}_2$  treatment of the H-terminated Si surface. The excellent electrical properties of Si in contact with alcoholic solutions of halogens have therefore generally been ascribed to the formation of Si-X ( $X = \text{I}$  or  $\text{Br}$ ) bonds.<sup>42-44</sup> Halogen-alcohol passivation of H-terminated Si has also been used for diagnostic measurements of bulk charge-carrier lifetimes in Si crystals<sup>43,45,60</sup> and for production of metal-silicon devices that have properties that differ from those formed from conventional metal-oxide-silicon junctions.<sup>61-68</sup> There is thus significant interest from a device performance perspective in understanding the chemistry of Si in alcohol solutions with and without the presence of a mild oxidizing agent.

Another related system of interest involves the use of Si/alcohol junctions as photoelectrochemical cells for the conversion of solar energy into electrical energy.<sup>69-72</sup> Work in our laboratory has shown that n-type Si/ $\text{CH}_3\text{OH}-\text{Me}_2\text{Fc}^{+/0}$  contacts (where  $\text{Me}_2\text{Fc}$  is 1,1'-dimethylferrocene) show excellent electrochemical behavior, exhibiting low surface recombination velocities,<sup>69,73,74</sup> high open circuit voltages,<sup>69,74</sup> and energy conversion efficiencies in unoptimized device configurations in excess of 14% under simulated solar illumination.<sup>70</sup> Exposure of n-Si to  $\text{CH}_3\text{OH}-\text{Me}_2\text{Fc}^{+/0}$  or to  $\text{CH}_3\text{OH}-\text{FcBF}_4$  solutions has been shown to produce a shift in the flat-band potential of n-Si/ $\text{CH}_3\text{OH}$  contacts,<sup>69,75</sup> presumably indicating some change in the state of the surface. Such changes have not been observed when n-Si is in contact with  $\text{CH}_3\text{OH}$  or  $\text{CH}_3\text{OH}$  that contains an inert electrolyte or a redox species with a less positive electrochemical potential than  $\text{Me}_2\text{Fc}^{+/0}$ .<sup>69</sup> Chazalviel has presented infrared spectroscopic evidence that exposure of 40% HF(aq) etched, H-terminated Si(111) surfaces to  $\text{CH}_3\text{OH}$  vapor produces a much reduced intensity of the Si-H stretching region and produces new peaks in the C-H stretching region of the infrared spectrum.<sup>76</sup> A shift in the flat-band potential was observed for such systems, similar to the flat-band shift that has been observed for H-terminated Si(100) surfaces after photoelectrochemical treatment in  $\text{CH}_3\text{OH}-\text{Me}_2\text{Fc}^{+/0}$ .<sup>69,76</sup> Also, anodization reactions of porous Si in methanol have been shown to produce a reduction in intensity of the infrared Si-H peak and to produce concomitant formation of Si-OCH<sub>3</sub> bonds.<sup>77</sup> A recent report from our laboratory is consistent with these observations and indicates that the (111)-oriented Si surface forms Si-OCH<sub>3</sub> groups after contact with  $\text{FcBF}_4$ ,  $\text{I}_2$ , and  $\text{Br}_2$  solutions in  $\text{CH}_3\text{OH}$ .<sup>26</sup>

In this work, we report the results of a series of infrared (IR) and X-ray photoelectron (XP) spectroscopic studies of crystalline Si surfaces after contact with various alcohol solutions. The (111)-oriented Si surface is of interest because it is relatively well-defined chemically,<sup>48-51</sup> while the (100)-oriented surface is of interest because it is the face used currently in most Si-based electronic devices.<sup>35</sup> The chemical treatments investigated in our work include exposure to unlabeled, deuterated, and fluorinated alcohols, with and without the presence of mild oxidizing agents. These studies have allowed us to relate the electronic properties of the Si surface to its chemical state under a variety of conditions of interest in electrical and electrochemical device fabrication.

## II. Experimental Section

**A. Instrumentation.** 1. *Surface Infrared Spectroscopy.* Surface infrared spectra were collected using a Mattson Galaxy

series (4326 upgrade) Polaris FT-IR spectrometer. The optical path consisted of custom-assembled external optics that included mirrors (Janos), a KRS-5 polarizer (Graseby Specac), a sample stage, and a detector (EG&G Judson). The optics were housed in a custom-built polycarbonate chamber that was continuously purged with dry nitrogen. Parallel concentric indium antimonide (InSb) and mercury cadmium telluride (MCT) detectors were used. The InSb detector was used for the 4000–1800  $\text{cm}^{-1}$  region and the MCT detector was used for the 1800–800  $\text{cm}^{-1}$  region. Both detectors were mounted in a single dewar flask. Spectra were collected at 1  $\text{cm}^{-1}$  resolution in attenuated total multiple internal reflection (ATR) mode. Data collection and analysis were performed on a PC using the WinFirst software package.

2. *X-ray Photoelectron Spectroscopy (XPS).* XPS data were collected using an M-probe spectrometer (VG Instruments) pumped by a CTI Cryogenics-8 cryo pump. The crystals were irradiated with monochromatic Al K $\alpha$  X-rays (1486.6 eV) that were incident at 35° from the sample surface. Photoelectrons were analyzed by a hemispherical analyzer mounted at a takeoff angle of 35° from the sample surface, and the incident X-rays and the electron analyzer axis were in vertical planes at right angles to each other. The crystals were mounted with gold-plated molybdenum clips onto a custom-made stainless steel stub. A groove was machined into the stub so that the ATR crystals could be suspended by two corners, thereby preventing the bottom surface of the crystal from contacting the stub. The samples were sufficiently conductive that all reported energy measurements are referenced to the Fermi level of the spectrometer.

Data collection and analysis were performed using M-probe software version 3.4. Two types of spectra were collected; the “survey scan” was collected in scanned mode, while the “high-resolution scans” were collected in unscanned mode. For both modes, an elliptical spot of dimensions 800  $\mu\text{m} \times 1200 \mu\text{m}$  was incident on the sample surface. The pass energy, energy window, and resolution (full width at half-maximum for Au 4f<sub>7/2</sub> peak) values were 154.7, 21.45, and  $1.50 \pm 0.01$  eV, respectively, for the survey mode and were 53.98, 6.85, and  $1.00 \pm 0.01$  eV, respectively, for the high-resolution mode. Typically, at each analyzed spot on the sample, a survey scan was collected from 0 to 1000 eV binding energy, followed by collection of a high-resolution scan of the Si 2p region (98.6–105.4 eV), followed (in some cases) by collection of a high-resolution scan of the C 1s (282–296 eV) region. All sensitivity factors and peak positions were normalized to the C 1s peak, which was assumed to have an intensity of 1.00 and a binding of 284.6 eV.

Quantification of surface coverages from the XP survey spectra was performed using the simple substrate-overlayer model<sup>78</sup> of eq 1:

$$\frac{I_{\text{ov}}}{I_{\text{Si}}} = \left( \frac{\text{SF}_{\text{ov}}}{\text{SF}_{\text{Si}}} \right) \left( \frac{\rho_{\text{ov}}}{\rho_{\text{Si}}} \right) \left[ \frac{1 - \exp\left(-\frac{d_{\text{ov}}}{\lambda_{\text{ov}} \sin \theta}\right)}{\exp\left(-\frac{d_{\text{ov}}}{\lambda_{\text{Si}} \sin \theta}\right)} \right] \quad (1)$$

In this equation,  $I_{\text{ov}}/I_{\text{Si}}$  is the raw intensity ratio of the overlayer element peak area to the Si 2p peak area, and  $\text{SF}_{\text{ov}}$  and  $\text{SF}_{\text{Si}}$  are the modified sensitivity factors for the overlayer atoms and for the substrate silicon atoms, respectively. The quantity  $\rho_{\text{Si}}$  is the density of the substrate silicon ( $8.30 \times 10^{-2} \text{ mol cm}^{-3}$ ),  $\rho_{\text{ov}}$  is the density of the atoms in the overlayer of interest,  $d_{\text{ov}}$  is the thickness of the overlayer that partially attenuates photo-

electrons that are emitted from the underlying substrate and from the overlayer,  $\lambda_{ov}$  and  $\lambda_{Si}$  are the escape depths through the overlayer for electrons of the relevant energy originating from orbitals in the overlayer and substrate, respectively, and  $\theta$  is the takeoff angle from the horizontal used in collection of the XPS data ( $35^\circ$ ).

Equation 1 can be rearranged to yield

$$\left(\frac{I_{ov}}{I_{Si}}\right)\left(\frac{SF_{Si}}{SF_{ov}}\right)\left(\frac{\rho_{Si}}{\rho_{ov}}\right) = \exp\left(\frac{d_{ov}}{\lambda_{Si} \sin \theta}\right) - \exp\left[\left(-\frac{d_{ov}}{\lambda_{ov} \sin \theta}\right) + \left(\frac{d_{ov}}{\lambda_{Si} \sin \theta}\right)\right] \quad (2)$$

When  $\lambda_{Si} = \lambda_{ov}$ , the last exponential term equals zero, in which case simplification and rearrangement yields

$$\ln\left[\left(\frac{I_{ov}}{I_{Si}}\right)\left(\frac{SF_{Si}}{SF_{ov}}\right)\left(\frac{\rho_{Si}}{\rho_{ov}}\right) + 1\right] \lambda \sin \theta = d_{ov} \quad (3)$$

When Si is covered by a fractional monolayer,  $\Phi_{ov}$ , an alternative formulation is<sup>78</sup>

$$\frac{\Phi_{ov}\{1 - \exp[-a_{ov}/(\lambda_{ov} \sin \theta)]\}}{1 - \Phi_{ov}\{1 - \exp[-a_{ov}/(\lambda_{Si} \sin \theta)]\}} \left(\frac{SF_{ov}}{SF_{Si}}\right)\left(\frac{\rho_{ov}}{\rho_{Si}}\right) = \left(\frac{I_{ov}}{I_{Si}}\right) \quad (4)$$

where  $a_{ov}$  is the atomic diameter of the species in the overlayer. If the photoelectron peaks are at high energy (so that  $\lambda_{Si} \cong \lambda_{ov}$ ) and  $\Phi_{ov}$  is small, eq 4 can be simplified and rearranged to<sup>78</sup>

$$\Phi_{ov} = \left[\frac{\lambda \sin \theta}{a_{ov}}\right] \left(\frac{SF_{Si}}{SF_{ov}}\right)\left(\frac{\rho_{Si}}{\rho_{ov}}\right)\left(\frac{I_{ov}}{I_{Si}}\right) \quad (5)$$

For the overlayers evaluated in this study, the surface coverages of fractional monolayers of F, Cl, Br, I, and O calculated using eq 3 or eq 5 were nearly identical.

The modified sensitivity factors were calculated according to eq 6

$$SF_{mod} = SF_{Scof} \left[\frac{1486 - BE}{1486 - 284}\right]^{S_{exp}} \quad (6)$$

as provided in the M-probe package software, where  $SF_{Scof}$  is the unmodified Scofield factor<sup>79</sup> and  $S_{exp}$  is the sensitivity exponent (0.65 for the survey scans and 0.6 for the high-resolution scans). This produced values for  $SF_{ov}$  of C 1s = 1.00, F 1s = 3.40, Cl 2s = 1.70, Br 3d = 2.84, I 4d = 4.688, O 1s = 2.52<sup>78</sup> and produced a value for  $SF_{Si}$  (Si 2p) of 0.90.

The coverages of elements in overlayers were calculated assuming that the overlayer consisted of the atom of interest packed with a density equal to the molar volume of that element in its solid-state form and having a monolayer thickness equal to the estimated atomic diameter of that element in the solid state. The molar volumes in the solid state of the halogens and of oxygen (F = 11.2 cm<sup>3</sup> mol<sup>-1</sup>; Cl = 17.4 cm<sup>3</sup> mol<sup>-1</sup>; Br = 19.8 cm<sup>3</sup> mol<sup>-1</sup>; I = 25.7 cm<sup>3</sup> mol<sup>-1</sup>; O = 17.4 cm<sup>3</sup> mol<sup>-1</sup>)<sup>80</sup> were used to compute the atomic number densities (F = 5.28 × 10<sup>22</sup> atoms cm<sup>-3</sup>; Cl = 3.43 × 10<sup>22</sup> atoms cm<sup>-3</sup>; Br = 3.04 × 10<sup>22</sup> atoms cm<sup>-3</sup>; I = 2.34 × 10<sup>22</sup> atoms cm<sup>-3</sup>; O = 3.46 × 10<sup>22</sup> atoms cm<sup>-3</sup>) for each of these atoms in their elemental solid-state form.<sup>78</sup> The atomic diameter,  $a$ , for each of these elements was then approximated by taking the inverse cube root of the atomic number density, producing atomic diameters of F = 0.26 nm, Cl = 0.31 nm, Br = 0.32 nm, I = 0.35 nm, and O = 0.31 nm. The thicknesses of the atomic overlayers

calculated using eq 3 were thus converted to fractional monolayer coverages by dividing the calculated overlayer thickness by the estimated atomic diameter of the atom forming the overlayer. Molar densities for overlayers of either bound or adventitious hydrocarbon<sup>81</sup> were estimated to be 3.3 × 10<sup>-2</sup> mol cm<sup>-3</sup> and the thickness of a monolayer of each of these types of hydrocarbon was taken to be 0.48 nm.<sup>81</sup>

The use of eqs 3 or 5, as opposed to eqs 1 or 4, respectively, was justified through analysis of XPS signals arising from overlayer element peaks that were close in energy to the Si 2p peak (C 1s, F 1s, Cl 2s, Br 3d<sub>3/2</sub>, O 1s, and I 4d), so that  $\lambda_{ov} \cong \lambda_{Si}$ . The escape depths of photoelectrons through the halogen or oxygen overlayers can be approximated using the empirical equation<sup>78</sup>

$$\lambda = 0.41a^{1.5}E^{0.5} \quad (7)$$

where  $E$  is the electron kinetic energy (in eV),  $\lambda$  is the attenuation length (in nm), and  $a$  is the diameter of the atoms in the monolayer (in nm). Through the use of eq 7,  $\lambda_{ov}$  was calculated to be 1.6 nm for F, 2.4 nm for Cl, 2.8 nm for Br, 3.2 nm for I, and 2.2 nm for O overlayers, while  $\lambda_{Si}$  was calculated to be 2.1, 2.6, 2.7, 3.2, and 2.6 nm for F, Cl, Br, I, and O overlayers, respectively. The attenuation lengths through the adventitious hydrocarbon overlayer for electrons originating in the C 1s level (3.9 nm) and for electrons originating in the Si 2p level (3.5 nm) were assumed to be the same as the values observed for long-chain thiols.<sup>81,82</sup> The approximation  $\lambda_{ov} \cong \lambda_{Si}$  is well-justified for overlayers composed of either C, Cl, Br, or I but is not as accurate for overlayers composed of F or O. Nevertheless, this approximation was made throughout to simplify the calculations.

The coverage of oxidized Si was calculated separately using two different methods to analyze the high-resolution XPS data in the Si 2p region. In the first method, the system was modeled as bulk Si covered with a thin SiO<sub>2</sub> overlayer. The thickness of the SiO<sub>2</sub> overlayer was calculated from the relative areas of the bulk Si 2p and oxidized Si 2p peaks in the high-resolution XP spectra through use of a simple substrate-overlayer model, as previously described.<sup>78,83</sup>

$$d = \lambda_{ov} \sin \theta \left\{ \ln \left[ 1 + \left( \frac{I_{Si}^o}{I_{Si}^p} \right) \left( \frac{I_{ov}}{I_{Si}} \right) \right] \right\} \quad (8)$$

In this equation,  $d$  is the overlayer thickness,  $\lambda_{ov}$  is the attenuation factor through the oxide overlayer (taken to be 2.6 nm),<sup>84</sup>  $\theta$  is the angle from the surface of the sample to the detector ( $35^\circ$ ), and  $I_{Si}^o/I_{Si}^p$  is an instrumental normalization factor related to the ratio of the signals expected for pure Si vs pure SiO<sub>2</sub> (determined to be 1.3 for our instrument).<sup>83</sup> The coverage was then calculated taking the thickness of a monolayer of SiO<sub>2</sub> to be 0.35 nm. The coverage of oxidized Si atoms on chlorinated Si surfaces was calculated similarly, so the fractional coverages of oxidized Si quoted for the chlorinated surfaces are equivalent coverages of oxidized Si at the Si/SiO<sub>2</sub> interface.

In the second method, the system is modeled as a flat Si-(111) or Si(100) surface, terminated with alkoxy groups or halogen atoms. Because the photoelectrons arising from the surface Si atoms and from the bulk Si atoms are very similar in energy, these photoelectrons are nearly identically attenuated by the overlayer alkoxy groups, halogen atoms, and adventitious hydrocarbon. Thus, the signal attenuation by any overlayer is nearly identical for photoelectrons arising from both the substrate

and overlayer, and the attenuation factors can therefore be ignored.<sup>88</sup> This treatment assumes that the scattering cross sections of the bulk Si and partially oxidized surface Si atoms are identical (a reasonable approximation with the X-ray energies used and for the oxidation states of Si of interest),<sup>86,88</sup> that the mean free path of the incident X-rays is much greater than the mean free path of the photoelectrons,<sup>89</sup> that electron refraction and reflection at the surface is negligible,<sup>89</sup> and that single-crystal effects are negligible.<sup>89</sup> These are all quite reasonable assumptions for the system of interest.

In this method, the coverage of oxidized Si can be straightforwardly calculated from the relative areas of the bulk Si 2p and oxidized Si 2p peaks observed in the high-resolution XP spectra. The total Si 2p signal is given by eq 9:

$$I_{\text{Si}} \approx n_{\text{Si}} \sigma_{\text{Si}} \int_0^{\infty} \exp(-z/l_{\text{Si}}) dz = n_{\text{Si}} \sigma_{\text{Si}} l_{\text{Si}} \quad (9)$$

where  $n_{\text{Si}}$  is the atomic number density of Si atoms ( $5.0 \times 10^{22}$  atoms  $\text{cm}^{-3}$ ),<sup>85</sup>  $\sigma_{\text{Si}}$  is the atomic photoionization cross section of Si, and the escape depth,  $l_{\text{Si}}$ , equals  $\lambda_{\text{Si}} \sin(35^\circ)$  with  $\lambda_{\text{Si}} = 1.6 \text{ nm}$ <sup>84</sup> and  $35^\circ$  representing the takeoff angle of electrons from the surface in our XPS instrument. The Si 2p signal arising from the oxidized surface Si atoms is given by eq 10:

$$I_{\text{Si,surf}} \approx n_{\text{Si,surf}} \sigma_{\text{Si}} \quad (10)$$

where  $n_{\text{Si,surf}}$  is the surface density of Si atoms ( $7.8 \times 10^{14}$  atoms  $\text{cm}^{-2}$  for Si(111) and  $6.9 \times 10^{14}$  atoms  $\text{cm}^{-2}$  for Si(100)).<sup>90</sup> If 100% of the surface Si atoms are oxidized, then the relative intensity of the oxidized Si peak to the bulk Si peak is given by eq 11:

$$\frac{I_{\text{Si(surf)}}}{I_{\text{Si(bulk)}}} = \frac{n_{\text{Si,surf}} \sigma_{\text{Si}}}{n_{\text{Si}} \sigma_{\text{Si}} l_{\text{Si}} - n_{\text{Si,surf}} \sigma_{\text{Si}}} = \frac{n_{\text{Si,surf}}}{n_{\text{Si}} l_{\text{Si}} - n_{\text{Si,surf}}} \quad (11)$$

Substituting into eq 11 yields a ratio of 0.21 for Si(111) and a ratio of 0.18 for Si(100) surfaces for which 100% of the surface Si atoms are oxidized and exhibit a peak at higher binding energy than that of the bulk Si 2p peak. The observed oxidized/bulk Si 2p peak area ratios were therefore divided by these normalization constants to estimate the fraction of surface atoms that were oxidized on the different crystal orientations studied in this work. This method was applied to oxidized Si atoms that were produced by forming either Si–O or Si–Cl bonds, depending on the specific reaction chemistry to which the surface had been exposed.

In both methods, the Si 2p peak arising from bulk Si was fit with two peaks (Si 2p<sub>1/2</sub> and Si 2p<sub>3/2</sub> peaks), while the oxidized Si peak was fit with a single peak. The Si 2p<sub>1/2</sub> to Si 2p<sub>3/2</sub> peak area ratio was fixed at 0.51, and the energy separation was fixed at 0.6 eV.<sup>85–87</sup> The small deviation from the statistical branching ratio of 0.50 has been attributed to slight differences in the final-state densities at the different energies of detection.<sup>85</sup> The peaks were best fit using 95% Gaussian/5% Lorentzian line shapes with a 15% peak asymmetry, where the asymmetry is introduced by assigning different line widths to the left- and right-hand sides of the peak, respectively. Because XPS is not sensitive to isotopic composition, the data for reactions that differed only through substitution of deuterium for hydrogen were averaged together to produce the summary tables presented herein of the peak intensities and derived coverages for each different surface/electrolyte combination of interest.

**B. General Procedures.** Single-crystal silicon attenuated total internal reflectance (ATR) IR plates were purchased from Harrick Scientific (Ossining, NY). The samples were trapezoidal

(1 mm × 50 mm × 20 mm) crystals with either (100)- or (111)-oriented faces that had beveled edges cut at 45° from the large faces. All data are displayed as absolute absorbances produced by the 50 optical reflections in these ATR crystals. Before each use, the crystals were chemically oxidized in 3:1 (v/v) concentrated H<sub>2</sub>SO<sub>4</sub>/40% H<sub>2</sub>O<sub>2</sub>(aq) at 100 °C for 1 h. Ferrocene (Fc, Aldrich or Strem) was purified by sublimation and was stored under N<sub>2</sub>(g). Ferrocenium tetrafluoroborate (FcBF<sub>4</sub>, Aldrich), phosphorus pentachloride (PCl<sub>5</sub>, Aldrich), benzoyl peroxide (Aldrich), and anhydrous CD<sub>3</sub>OD (Aldrich) were used as received and were stored under N<sub>2</sub>(g). Anhydrous methanol (Aldrich), chlorobenzene (C<sub>6</sub>H<sub>5</sub>Cl, Aldrich), and tetrahydrofuran (THF, Aldrich) were stored under N<sub>2</sub>(g) over activated 3 Å molecular sieves (VWR). The functionalized crystals were transferred between the UHV system and the N<sub>2</sub>(g)-purged IR chamber by taking the specimens into the N<sub>2</sub>-filled glovebox that was attached to the UHV system and placing the samples in a jar the lid of which was tightly closed and sealed with electrical tape. The jar was transferred to the IR chamber via a quick entry port and the chamber was then purged with a rapid flow of N<sub>2</sub>(g) for 20 min before the specimen was removed from the jar and mounted in the IR beam. The specimens were similarly transferred back to the glovebox and UHV chamber in a sealed jar.

**1. Spectra of H-Terminated Si Surfaces Exposed to Alcohols and to FcBF<sub>4</sub>-, I<sub>2</sub>-, and Br<sub>2</sub>-Alcohol Solutions.** IR backgrounds were collected using freshly oxidized Si ATR plates. Background spectra were obtained with the InSb (1800–4000  $\text{cm}^{-1}$ ) detector using s-polarized light and separately with p-polarized light. The (111)-oriented crystals were etched in N<sub>2</sub>-sparged 40% NH<sub>4</sub>F(aq) (Transene Inc.) until the p-polarized spectrum, measured relative to the p-polarized oxidized Si background spectrum, displayed a sharp silicon monohydride peak at 2083  $\text{cm}^{-1}$  superimposed on small, broad peaks arising from SiH<sub>2</sub> and SiH<sub>3</sub>. The sharp Si–H monohydride peak was always large in crystals that were considered sufficiently etched for subsequent reaction. In a few cases, only the sharp monohydride peak could be detected in the p-polarized spectra, but usually this sharp feature was superimposed on the broader peaks arising from di- and trihydride species. Typically, >40% of the integrated intensity was contained in the sharp monohydride peak. The (100)-oriented crystals were etched in N<sub>2</sub>-sparged 48% HF(aq) (VWR) for 0.5–2 min.

A Si crystal with a satisfactory IR spectrum was then transferred to UHV, and XP spectra were collected at three spots on the crystal. If any oxidation was detectable in the Si 2p region of the XP spectrum, the crystal was re-etched and the entire IR/XPS process was repeated. Crystals with satisfactory IR and XP spectra were then transferred from UHV directly into a N<sub>2</sub>-purged glovebox (Vacuum Atmospheres Inc.), in which all subsequent wet chemistry was performed. Unless otherwise specified, all IR spectra displayed in the figures are referenced to the oxidized Si ATR plate as a background.

To explore the chemistry of these surfaces, a H-terminated Si ATR crystal was exposed to CH<sub>3</sub>OH or CD<sub>3</sub>OD for 2–5 min and was washed in THF and dried under a stream of pressurized N<sub>2</sub>(g). The sample was transferred, in a jar, to the IR apparatus, and two separate IR spectra were collected over the 4000–1800  $\text{cm}^{-1}$  wavelength range, with each spectrum being obtained in both s- and p-polarizations. In the first run, the spectra acquired in the s-polarization and then in the p-polarization were referenced to the corresponding spectra of the freshly oxidized Si ATR plate. In the second run, the collected spectra were referenced to the corresponding spectra

of the ATR plate after it had been H-terminated (by etching in  $\text{NH}_4\text{F}(\text{aq})$ , vide supra). The Si ATR plate was then immersed for 2 min in a solution that had been freshly saturated ( $<30$  min old) with Fc in either  $\text{CH}_3\text{OH}$  or  $\text{CD}_3\text{OD}$ , and the crystal was washed in THF and dried under flowing  $\text{N}_2(\text{g})$ . Two sets of ( $4000\text{--}1800\text{ cm}^{-1}$ ) IR spectra, one relative to the spectra of the oxidized ATR plate and the other relative to the spectra of the H-terminated ATR plate, each obtained in s-polarization and then in p-polarization, were collected. The sample was then immersed for 2 min in a fresh ( $\sim 30$  min old)  $\text{CH}_3\text{OH}$  or  $\text{CD}_3\text{OD}$  solution that had been saturated with  $\text{FcBF}_4$ . Two sets of IR spectra were collected on this sample as well, each in both s- and p-polarization. The ATR plate was then transferred to UHV and XP spectra were collected in survey scan and high-resolution modes.

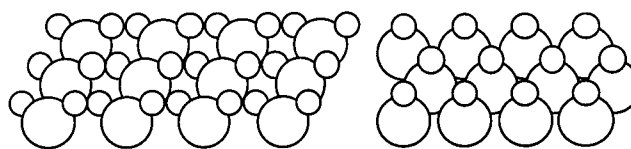
The surface chemistry of the Si ATR plates was further investigated using  $\text{CH}_3\text{OH}$  or  $\text{CD}_3\text{OD}$  solutions that contained either  $\text{I}_2$  or  $\text{Br}_2$ . Hydrogen-terminated Si crystals were obtained and characterized as described above and were then immersed for 15 min into a fresh ( $\sim 30$  min old)  $\text{CH}_3\text{OH}$  or  $\text{CD}_3\text{OD}$  solution that contained  $10\text{--}150\text{ mM}$   $\text{I}_2$  or  $200\text{--}300\text{ mM}$   $\text{Br}_2$ . The crystal was washed in  $\text{CH}_3\text{OH}$  (or  $\text{CD}_3\text{OD}$ ) three times, then washed with THF followed by  $\text{CH}_3\text{CN}$ , dried with  $\text{N}_2$ , and transferred to UHV. XP spectra were then collected in survey scan and high-resolution modes. The crystal was then transferred to the IR chamber and two sets of IR spectra (from  $4000$  to  $1800\text{ cm}^{-1}$ ) were collected with the treated surface referenced to the oxidized and hydrogen-terminated surface in both s- and p-polarization.

The persistence of the residual I and Br on the surface and the exchangeability of the methoxylated surfaces was explored by immersing a H-terminated Si(111) or a H-terminated Si-(100) oriented ATR crystal for 5–15 min into a  $\text{CH}_3\text{OH}$  solution that contained  $\text{FcBF}_4$ ,  $\text{I}_2$ , or  $\text{Br}_2$  and then washing the crystal with  $\text{CD}_3\text{OD}$ , THF, and  $\text{CH}_3\text{CN}$  (crystals exposed to  $\text{CD}_3\text{OD}$  solution were washed with  $\text{CH}_3\text{OH}$ ). IR and XP spectra were then collected as described above to determine whether surficial I, Br, or  $-\text{OCH}_3$  groups had been replaced by  $-\text{OCD}_3$  groups during washing. After collection of the IR and XP spectra, the  $\text{FcBF}_4\text{--CH}_3\text{OH}$  treated crystals were then returned to the glovebox and contacted with  $\text{CD}_3\text{OD}$  for 2 h. IR and XP spectra were then collected.

The effect of exposing the Si ATR plates to longer-chain alcohols was also examined using  $\text{C}_4\text{D}_9\text{OD}$  and  $\text{C}_4\text{H}_9\text{OH}$  solutions. Hydrogen-terminated Si(111) crystals were produced by etching in  $\text{N}_2$ -sparged  $40\%$   $\text{NH}_4\text{F}(\text{aq})$ , and IR and XP spectra were collected as described above. Additional IR spectra were collected in s- and p-polarization (from  $4000$  to  $1800\text{ cm}^{-1}$ ) after the crystal was successively contacted with  $\text{C}_4\text{D}_9\text{OD}$  (or  $\text{C}_4\text{H}_9\text{OH}$ ) for 5 min, with Fc saturated in  $\text{C}_4\text{D}_9\text{OD}$ , and then with  $\text{FcBF}_4$  saturated in  $\text{C}_4\text{D}_9\text{OD}$ . After each of these treatments, the crystal was washed three times in the parent alcohol, once with THF, and once with  $\text{CH}_3\text{CN}$ , dried with a stream of  $\text{N}_2$ , and transferred to the IR chamber. After the series of exposures, the crystal was returned to UHV and XP spectra were collected.

The surface chemistry of the Si ATR plates was also studied using a fluorinated alcohol,  $\text{HO}(\text{CH}_2)_3\text{CF}_3$ , as the solvent. These experiments were of interest because F has a large XPS cross section and because the fluorinated carbon atom provides an XPS C 1s signal that is distinct from the C 1s signal arising from adventitious carbonaceous adsorbates. The procedures were generally as described above, except that XP spectra were collected after each wet chemical immersion step. The ATR sample was first immersed for 2–3 min in  $\text{HO}(\text{CH}_2)_3\text{CF}_3$  and

## SCHEME 1



was then washed with THF,  $\text{CH}_3\text{CN}$ , and  $\text{CH}_2\text{Cl}_2$  and dried with a stream of  $\text{N}_2(\text{g})$  before collection of IR and XP spectra. The crystal was then immersed for 5 min into a solution of  $\text{HO}(\text{CH}_2)_3\text{CF}_3$  that was saturated with Fc, after which the Si was rinsed with THF,  $\text{CH}_3\text{CN}$ , and  $\text{CH}_2\text{Cl}_2$  and dried with  $\text{N}_2(\text{g})$ . After collecting XP and IR spectra, the crystal was then contacted with  $\text{HO}(\text{CH}_2)_3\text{CF}_3\text{--Fc--FcBF}_4$  (prepared by adding the saturated Fc solution to solid  $\text{FcBF}_4$ ) for 4–5 min, washed in THF,  $\text{CH}_3\text{CN}$ , and  $\text{CH}_2\text{Cl}_2$ , and dried with a stream of  $\text{N}_2$ , IR spectra were collected, and the crystal was taken into UHV for XPS measurements.

**2. Two-Step Chlorination/Alkoxylation of H-Terminated Si Surfaces.** After obtaining satisfactory IR and XP spectra for H-terminated surfaces as described above, either (100)- or (111)-oriented Si crystals were placed in contact with a saturated solution of  $\text{PCl}_5$  solution in chlorobenzene to which a few grains of benzoyl peroxide had been added. The reaction was performed for 50–60 min at  $90\text{--}95\text{ }^\circ\text{C}$  in a glovebox. The crystals were then washed in  $\text{CH}_3\text{OH}$ , THF, and  $\text{CH}_3\text{CN}$ , dried with a stream of pressurized  $\text{N}_2(\text{g})$ , and taken into UHV. XPS data were collected, and then the crystals were exposed in the  $\text{N}_2(\text{g})$ -filled box to a lithium alkoxide solution. The lithium methoxides were prepared by addition of  $2.5\text{ M}$  n-butyllithium in hexanes to anhydrous  $\text{CH}_3\text{OH}$  or to anhydrous  $\text{CD}_3\text{OD}$ . The five combinations of crystal orientation and alkoxide (with reaction temperature and reaction time in parentheses) that were explored in this work were as follows: (100)-oriented Si with  $1\text{ M LiOCH}_3\text{--CH}_3\text{OH}$  ( $80\text{ }^\circ\text{C}$ ,  $21.5\text{ h}$ ), (100)-oriented Si with  $1\text{ M LiOCD}_3\text{--CD}_3\text{OD}$  ( $70\text{ }^\circ\text{C}$ ,  $23.5\text{ h}$ ), (111)-oriented Si with  $1\text{ M LiOCH}_3\text{--CH}_3\text{OH}$  ( $75\text{ }^\circ\text{C}$ ,  $19\text{ h}$ ), (111)-oriented Si with  $1\text{ M LiOCD}_3\text{--CD}_3\text{OD}$  ( $70\text{ }^\circ\text{C}$ ,  $19\text{ h}$ ), and (111)-oriented Si with  $1\text{ M LiO}(\text{CH}_2)_3\text{CF}_3\text{--THF}$  prepared by adding  $7.5\text{ mL}$  of  $2.5\text{ M LiC}_4\text{H}_9$  in hexanes to  $2.6\text{ mL}$  of  $\text{HO}(\text{CH}_2)_3\text{CF}_3$  in  $20\text{ mL}$  of THF ( $80\text{ }^\circ\text{C}$ ,  $15.5\text{ h}$ ). The  $\text{HO}(\text{CH}_2)_3\text{CF}_3\text{--THF--LiC}_4\text{H}_9$  solution turned from light yellow to deep orange-red before the ATR crystal was added. After treatment, the crystals were washed in  $\text{CH}_3\text{OH}$  ( $\text{CD}_3\text{OD}$ ), THF, and  $\text{CH}_3\text{CN}$  (the  $\text{LiO}(\text{CH}_2)_3\text{CF}_3$ -exposed crystal was washed in THF,  $\text{CH}_3\text{OH}$ ,  $\text{CH}_3\text{CN}$ , and  $\text{CH}_2\text{Cl}_2$ ) and dried with a stream of  $\text{N}_2(\text{g})$ . The ATR plates were then taken into UHV, and XP spectra were collected. Samples were then transferred to the IR apparatus and two sets of IR spectra, one referenced to the spectra of the oxidized Si ATR plate and the other referenced to the spectra of the H-terminated Si ATR plate, were obtained in both s- and p-polarization.

## III. Results

Because the etching of (111)-oriented Si by  $\text{NH}_4\text{F}(\text{aq})$  is known to produce a monohydride-terminated surface with large, atomically flat terraces,<sup>48–51</sup> most of the surface reactivity studies described herein were performed on this crystal face. Moreover, modeling of the packing of monolayers on the (111)-oriented surface is relatively straightforward because the Si–H bonds are arranged in a well-defined trigonal array and are oriented normal to the (111) surface plane (Scheme 1, right).<sup>91</sup> The chemistry of the (100)-oriented face (Scheme 1, left) was also studied because this surface is the technologically more important face of Si<sup>35</sup> and because the (100) orientation is the

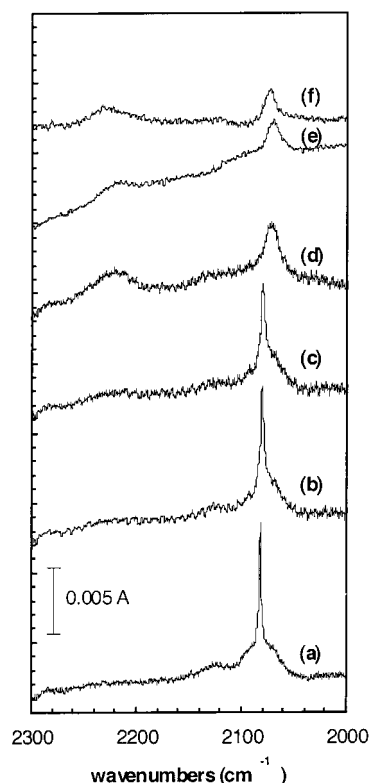


**Figure 1.** FT-IR spectra of a Si(111) ATR crystal after (a) etching in  $N_2$ -sparged 40%  $NH_4F(aq)$ , (b) immersion for 5 min in  $CD_3OD$ , (c) immersion for 3–5 min in  $CD_3OD$  containing 200 mM ferrocene, and (d) immersion for 3–5 min in  $CD_3OD$  containing 200 mM ferrocenium  $[BF_4]$ , and (e) a different H-terminated ATR crystal after immersion for 15 min in  $CD_3OD$  containing 25 mM  $I_2$  and (f) a different H-terminated ATR crystal after immersion for 15 min in  $CD_3OD$  containing 200 mM  $Br_2$ . The data are the total absorbance produced by 50 reflections within the crystal and are referenced to an oxidized Si crystal as the background spectrum.

face that has been used previously in most photoelectrochemical studies of n-type Si in contact with various electrolytes.<sup>69–72,75,92,93</sup>

#### A. Si(111) Surface Chemistry in Methanol Solutions. 1.

**Exposure to  $CD_3OD$ .** Figure 1 shows surface IR spectra in the 2000–2300  $cm^{-1}$  energy region of a (111)-oriented Si ATR crystal after etching and exposure to  $CD_3OD$  and then to various reagents in methanol. The Si surface was initially H-terminated after exposure to 40%  $NH_4F(aq)$ , as evidenced by the sharp, strongly p-polarized infrared stretch at 2083  $cm^{-1}$  in Figure 1a and by the absence of any detectable oxidized Si peaks in the Si 2p region of the XP spectrum of such samples (Figure 2). Immersing this Si sample in  $CD_3OD$  for 2–5 min (Figure 1b) and subsequently immersing it in saturated  $CD_3OD$ –200 mM Fc for 2 min (Figure 1c) produced some broadening of the 2083  $cm^{-1}$  Si–H infrared peak and some loss in intensity of this signal. The slight decrease in intensity was also observed over similar time periods when freshly etched (111)-oriented Si ATR crystals were placed in the IR beam and spectra were periodically collected without moving the crystal. As opposed to these generally subtle spectral changes, immersion of the Si into  $CD_3OD$  that had been saturated with  $FcBF_4$  (~200 mM  $FcBF_4$ ) produced significant changes in both the IR and XP spectra of such samples. The IR spectrum showed a complete loss of the sharp positive peak near 2083  $cm^{-1}$  (Figure 1d), while peaks at 2070  $cm^{-1}$  ( $\nu_s(CD_3)$ ) and 2225  $cm^{-1}$  ( $\nu_{as}(CD_3)$ ) appeared, consistent with the formation of surficial Si–OCD<sub>3</sub> groups. The observed peak positions closely match the established peak positions for the symmetric and asymmetric methyl stretches

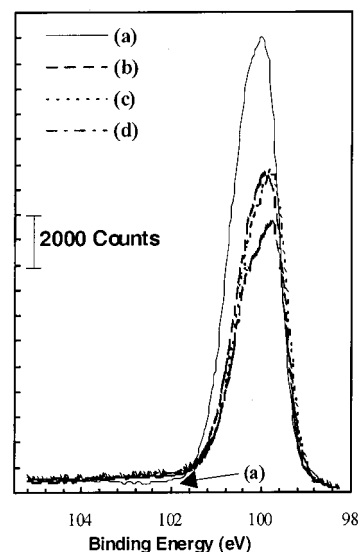


**Figure 2.** High-resolution Si 2p XP spectra of a Si(111) ATR crystal after (a) etching in  $N_2$ -sparged 40%  $NH_4F(aq)$  and (b) immersion for 3–5 min in  $CD_3OD$ , for 3–5 min in  $CD_3OD$  containing 200 mM ferrocene, and then for 3–5 min in  $CD_3OD$  containing 200 mM ferrocenium  $[BF_4]$  and (c) a different H-terminated ATR crystal after immersion for 15 min in  $CD_3OD$  containing 25 mM  $I_2$  and (d) a different H-terminated ATR crystal after immersion for 15 min in  $CD_3OD$  containing 200 mM  $Br_2$ . The XP spectra of surfaces exposed to  $CH_3OH$  solutions were identical to those obtained from surfaces exposed to the analogous  $CD_3OD$  solutions.

of gas-phase  $CD_3OD$  ( $\nu_s(CD_3)$  at 2080  $cm^{-1}$  and  $\nu_{as}(CD_3)$  at 2228  $cm^{-1}$ ).<sup>94</sup> In some samples, as much as 80% of the initial Si–H intensity was observed in the sharp Si–H peak, and after exposure to  $FcBF_4$ – $CH_3OH$  solutions, such samples showed somewhat larger intensities of the peaks ascribable to surficial Si–OCD<sub>3</sub> groups than are evident in the spectra depicted in Figure 1.

The high-resolution XP spectra of the Si 2p region of these surfaces exhibited a peak at higher binding energy than the main Si 2p peak (the oxidized Si signal in spectrum b of Figure 2 is small but clearly distinguishable from the baseline established by the XP spectrum of the freshly  $NH_4F$ -etched surface, spectrum a). The oxidized silicon signal was relatively narrow (~1.2 eV) and was centered at 102.1 eV binding energy. The area of the oxidized silicon peak was about 3% of the total Si intensity, corresponding to ~0.15 monolayers of oxidized silicon (Tables 1 and 2). Subsequent experiments in which the freshly etched H-terminated Si crystal was immersed only into a  $CH_3OH$ –200 mM  $FcBF_4$  solution showed similar changes in the IR and XP spectra to those of Figure 1d and Figure 2, demonstrating that the predominant spectral changes were associated with immersion in the methanolic  $Fc^+$  solution and were not the result of cumulative exposure to solutions or of other time-dependent changes in the surface of the crystals.

Changes very similar to those that occurred upon exposure to  $CD_3OD$  solutions containing  $FcBF_4$  were observed in the IR spectra of hydrogen-terminated ATR crystals that had been immersed for 15 min in  $CD_3OD$  solutions that contained either 25 mM  $I_2$  (Figure 1e) or 200 mM  $Br_2$  (Figure 1f). The silicon monohydride peak was completely eliminated, while peaks at 2070  $cm^{-1}$  ( $\nu_s(CD_3)$ ) and 2225  $cm^{-1}$  ( $\nu_{as}(CD_3)$ ) appeared, consistent with the formation of surficial Si–OCD<sub>3</sub> groups. The intensity of the  $CD_3$  peaks produced after exposure of the H-terminated Si(111) surface to  $CD_3OD$  solutions containing  $I_2$  or  $Br_2$  was ~50% of the peak intensity produced after exposure to the  $FcBF_4$  solution (Figure 1). Immersion in  $CD_3$ -

TABLE 1: XPS Peak Area Ratios and Overlayer Coverages for Si(111) Surfaces

reaction	Si 2s/Si 2p	C 1s/Si 2p	O 1s/Si 2p	O 1s/C 1s	F 1s/Si 2p	I 4d/Si 2p	I 3d <sub>5/2</sub> /Si 2p	I 3d <sub>3/2</sub> /Si 2p	Br 3d <sub>3/2</sub> /Si 2p	Cl 2s/Si 2p
40% NH <sub>4</sub> F	1.22 ± 0.03	0.24 ± 0.14	0.20 ± 0.11	0.75 ± 0.22	0.02 ± 0.04					
CH <sub>3</sub> OH–FcBF <sub>4</sub>	1.22 ± 0.03	0.41 ± 0.18	0.65 ± 0.11	1.73 ± 0.34	0.35 ± 0.23					
CH <sub>3</sub> OH–I <sub>2</sub>	1.22 ± 0.03	0.48 ± 0.06	0.68 ± 0.04	1.44 ± 0.13	0.01 ± 0.03	0.119 ± 0.010	0.59 ± 0.02	0.46 ± 0.02		
CH <sub>3</sub> OH–Br <sub>2</sub>	1.24 ± 0.03	0.42 ± 0.09	0.52 ± 0.04	1.18 ± 0.14					0.22 ± 0.02	
C <sub>4</sub> H <sub>9</sub> OH–FcBF <sub>4</sub>	1.21 ± 0.02	0.38 ± 0.03	0.47 ± 0.04	1.25 ± 0.07	0.15 ± 0.03					
HOC <sub>4</sub> H <sub>6</sub> F <sub>3</sub>	1.23 ± 0.02	0.29 ± 0.10	0.24 ± 0.13	0.82 ± 0.24	0.03 ± 0.04					
HOC <sub>4</sub> H <sub>6</sub> F <sub>3</sub> –Fc	1.23 ± 0.03	0.30 ± 0.05	0.25 ± 0.06	0.86 ± 0.20	0.08 ± 0.01					
HOC <sub>4</sub> H <sub>6</sub> F <sub>3</sub> –FcBF <sub>4</sub>	1.19 ± 0.01	0.39 ± 0.08	0.43 ± 0.17	1.17 ± 0.47	0.66 ± 0.27					
PCl <sub>5</sub>	1.22 ± 0.04	0.44 ± 0.11	0.35 ± 0.09	0.80 ± 0.20						0.27 ± 0.03
Si–Cl + LiOCH <sub>3</sub>	1.22 ± 0.02	0.36 ± 0.16	0.56 ± 0.32	1.46 ± 0.27						0 ± 0
Si–Cl + LiOC <sub>4</sub> H <sub>6</sub> F <sub>3</sub>	1.19 ± 0.03	0.98 ± 0.04	0.94 ± 0.03	0.956 ± 0.007	0.61 ± 0.19					0.18 ± 0.06

reaction	monolayers hydrocarbon (from C 1s/Si 2p) <sup>a</sup>	equivalent monolayers <sup>b</sup> O (from O 1s/Si 2p) <sup>b</sup>	monolayers <sup>c</sup> F (from F 1s/Si 2p) <sup>b</sup>	monolayers <sup>c</sup> I (from I 4d/Si 2p)	monolayers <sup>c</sup> Br (from Br 3d <sub>3/2</sub> /Si 2p) <sup>b</sup>	monolayers <sup>c</sup> Cl (from Cl 2s/Si 2p) <sup>b</sup>
40% NH <sub>4</sub> F	1.9	0.49	0.023			
CH <sub>3</sub> OH–FcBF <sub>4</sub>	2.7	1.4	0.40			
CH <sub>3</sub> OH–I <sub>2</sub>	3.1	1.4	0.011	0.26		
CH <sub>3</sub> OH–Br <sub>2</sub>	2.8	1.1			0.55	
C <sub>4</sub> H <sub>9</sub> OH–FcBF <sub>4</sub>	2.6	1.0	0.17			
HOC <sub>4</sub> H <sub>6</sub> F <sub>3</sub>	2.1	0.59	0.034			
HOC <sub>4</sub> H <sub>6</sub> F <sub>3</sub> –Fc	2.2	0.62	0.092			
HOC <sub>4</sub> H <sub>6</sub> F <sub>3</sub> –FcBF <sub>4</sub>	2.6	1.0	0.76			
PCl <sub>5</sub>	2.9	0.86				0.99
Si–Cl + LiOCH <sub>3</sub>	2.5	1.2				0
Si–Cl + LiOC <sub>4</sub> H <sub>6</sub> F <sub>3</sub>	4.9	1.9	0.79			0.66

<sup>a</sup> Calculated using eq 3,<sup>78</sup> where the sensitivity factors were 1.00 for C 1s and 0.90 for Si 2p, the escape depth of the Si 2p electron through the hydrocarbon overlayer was taken to be 3.5 nm,<sup>81,82</sup> the molar density of Si is  $8.30 \times 10^{-2} \text{ mol cm}^{-3}$ , the molar density of the overlayer was estimated to be  $3.3 \times 10^{-2} \text{ mol cm}^{-3}$ ,<sup>81</sup> and the thickness of a monolayer was taken to be 0.48 nm.<sup>81</sup> <sup>b</sup> Monolayer coverages  $\geq 1.0$  were calculated using eq 3 and monolayer coverages  $< 1.0$  were calculated using eq 5.<sup>78</sup> The sensitivity factors were 2.52 for O 1s and 0.90 for Si 2p,<sup>78,79</sup> the escape depth of the Si 2p electron through the overlayer was taken to be 2.6 nm,<sup>78</sup> the atomic density of Si is  $5.0 \times 10^{22} \text{ atoms cm}^{-3}$ , the atomic density of O is  $3.46 \times 10^{22} \text{ atoms cm}^{-3}$ ,<sup>80</sup> and the thickness of a monolayer ( $d_{\text{ov}}$  in eq 3 and  $a_{\text{ov}}$  in eq 5) is estimated as 0.31 nm.<sup>78</sup> <sup>c</sup> Monolayer coverages were calculated using eq 5,<sup>78</sup> where the sensitivity factors were 3.40 for F 1s, 1.70 for Cl 2s, 2.84 for Br 3d, 4.69 for I 4d, and 0.90 for Si 2p,<sup>78,79</sup> the escape depth of the Si 2p photoelectrons through the overlayer was taken to be 2.1, 2.6, 2.7, 2.7, and 3.2 nm for F, Cl, Br, and I, respectively,<sup>78</sup> the atomic densities (atoms  $\text{cm}^{-3}$ ) were  $F = 5.28 \times 10^{22}$ ,  $Cl = 3.43 \times 10^{22}$ ,  $Br = 3.04 \times 10^{22}$ ,  $I = 2.34 \times 10^{22}$ , and  $Si = 5.0 \times 10^{22}$ ,<sup>80</sup> and the atomic diameter of the atom forming the overlayer was estimated to be 0.26, 0.31, 0.32, and 0.35 nm for F, Cl, Br, and I, respectively.<sup>78</sup>

TABLE 2: Coverage of Oxidized Si from High-Resolution XPS of Si(111)

reaction	SiO <sub>x</sub> 2p/Si <sub>bulk</sub> 2p	% monolayer <sup>a</sup> SiO <sub>x</sub>	% monolayer <sup>b</sup> Si <sup>1+</sup>
40% NH <sub>4</sub> F etched	0 ± 0	0 ± 0	0 ± 0
CH <sub>3</sub> OH–FcBF <sub>4</sub>	0.029 ± 0.007	16 ± 4	14 ± 3
CH <sub>3</sub> OH–I <sub>2</sub>	0.022 ± 0.008	12 ± 4	10 ± 4
CH <sub>3</sub> OH–Br <sub>2</sub>	0.021 ± 0.013	11 ± 7	10 ± 6
C <sub>4</sub> H <sub>9</sub> OH–FcBF <sub>4</sub>	0.014 ± 0.008	8 ± 4	7 ± 4
C <sub>6</sub> H <sub>5</sub> Cl–PCl <sub>5</sub>	0.045 ± 0.009	24 ± 5	21 ± 4
Si–Cl + LiOCH <sub>3</sub>	0.024 ± 0.005	13 ± 3	11 ± 2
HOC <sub>4</sub> H <sub>6</sub> F <sub>3</sub>	0 ± 0	0 ± 0	0 ± 0
HOC <sub>4</sub> H <sub>6</sub> F <sub>3</sub> –Fc	0 ± 0	0 ± 0	0 ± 0
HOC <sub>4</sub> H <sub>6</sub> F <sub>3</sub> –FcBF <sub>4</sub>	0.04 ± 0.02	22 ± 9	19 ± 9
Si–Cl + LiOC <sub>4</sub> H <sub>6</sub> F <sub>3</sub>	0.041 ± 0.001	22.2 ± 0.7	20 ± 0.5

<sup>a</sup> Calculated using eq 8, where the escape depth of the Si 2p electron through an oxide overlayer was taken to be 2.6 nm,<sup>84</sup>  $\theta = 35^\circ$ , the peak ratio of pure Si to pure SiO<sub>2</sub> ( $I_{\text{Si}}^0/I_{\text{Ov}}^0$ ) in the Si 2p region is determined to be 1.3,<sup>83</sup> and the thickness of a monolayer of SiO<sub>2</sub> was estimated to be 0.35 nm.<sup>83</sup> <sup>b</sup> Calculated using eq 11, in which 21% of the total unattenuated photoelectrons are calculated to originate from the surface atoms ( $7.8 \times 10^{14} \text{ atoms cm}^{-2}$ ) on Si(111). The ratio of the Si 2p peak arising from oxidized Si to the Si 2p peak arising from bulk Si was divided by 0.21 to determine the fraction of surficial Si atoms in an oxidized state.

OD–FcBF<sub>4</sub> (three trials) produced integrated peak intensities of  $0.060 \pm 0.007$  ( $\nu_s(\text{CD}_3)$ ) and  $0.057 \pm 0.009$  ( $\nu_{\text{as}}(\text{CD}_3)$ ), compared to integrated intensities of  $0.033 \pm 0.007$  ( $\nu_s(\text{CD}_3)$ ) and  $0.028 \pm 0.009$  ( $\nu_{\text{as}}(\text{CD}_3)$ ) following immersion in CD<sub>3</sub>OD–I<sub>2</sub> (two trials) and integrated intensities of  $0.025 \pm 0.015$  ( $\nu_s(\text{CD}_3)$ ) and  $0.029 \pm 0.024$  ( $\nu_{\text{as}}(\text{CD}_3)$ ) following immersion in

CD<sub>3</sub>OD–Br<sub>2</sub> (two trials). This smaller peak intensity occurred despite the longer immersion time in the I<sub>2</sub> and Br<sub>2</sub> solutions.

The high-resolution XP spectra collected on the surfaces exposed to I<sub>2</sub>–methanol or Br<sub>2</sub>–methanol solutions were similar to those produced by FcBF<sub>4</sub>–methanol exposed surfaces (Figure 2, Tables 1 and 2). The oxidized Si peak observed in the Si 2p region was similar in size, shape, and position to that obtained after exposure to FcBF<sub>4</sub> in CD<sub>3</sub>OD (Figure 2c,d, Table 2), suggesting that a similar surface species and surface coverage was obtained after the I<sub>2</sub>–CD<sub>3</sub>OD and Br<sub>2</sub>–CD<sub>3</sub>OD treatments. However, as seen in the survey scan XP spectra (Figure 3, Table 1), the surfaces produced by these three treatments are not identical. The surface exposed to FcBF<sub>4</sub>–CD<sub>3</sub>OD exhibited a F 1s peak corresponding to 40% of a monolayer of F atoms,<sup>95</sup> the surface exposed to I<sub>2</sub>–CD<sub>3</sub>OD exhibited an I peak corresponding to approximately 25% of a monolayer of I atoms, and the surface exposed to Br<sub>2</sub>–CD<sub>3</sub>OD exhibited a Br peak corresponding to approximately 55% of a monolayer of Br atoms. These observations are consistent with the hypothesis that exposure of H-terminated Si to alcoholic solutions of halogens produces surfaces that have a mixture of silicon–alkoxide and silicon–halogen surface bonding. In addition, the hydrocarbon coverage increased from approximately 1.9 monolayers on the freshly etched surfaces to approximately 2.7, 3.1, and 2.8 monolayers after immersion in CD<sub>3</sub>OD–FcBF<sub>4</sub>, CD<sub>3</sub>OD–I<sub>2</sub>, or CD<sub>3</sub>OD–Br<sub>2</sub>, respectively (Table 1). The ratio of the O 1s peak area to the C 1s peak area increased from  $\sim 0.8$  on the NH<sub>4</sub>F-etched surface to  $\sim 1.4$  on surfaces exposed to either CD<sub>3</sub>OD–FcBF<sub>4</sub>, CD<sub>3</sub>OD–I<sub>2</sub>, or CD<sub>3</sub>OD–Br<sub>2</sub> (Table 1), which is consistent with expectations for the formation of covalently

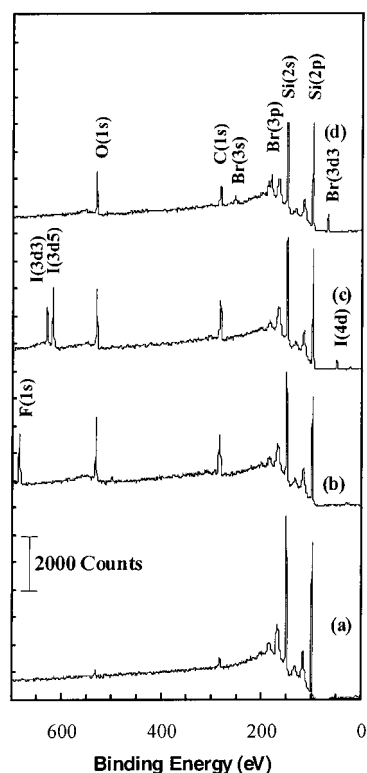


**Figure 3.** XP survey spectra of a Si(111) ATR crystal after (a) etching in  $N_2$ -sparged 40%  $NH_4F(aq)$  and (b) immersion for 3–5 min in  $CD_3OD$ , for 3–5 min in  $CD_3OD$  containing 200 mM ferrocene, and for 3–5 min in  $CD_3OD$  containing 200 mM ferrocenium  $[BF_4]$  and (c) a different H-terminated ATR crystal after immersion for 15 min in  $CD_3OD$  containing 25 mM  $I_2$  and (d) a different H-terminated ATR crystal after immersion for 15 min in  $CD_3OD$  containing 200 mM  $Br_2$ . These spectra were obtained on the same samples that were used to collect the data of Figure 1. The XP spectra of surfaces exposed to  $CH_3OH$  solutions were identical to those obtained from surfaces exposed to the analogous  $CD_3OD$  solutions.

attached methoxide groups in addition to presence of adventitious adsorbed hydrocarbon.

**2. Exposure to  $CH_3OH$ .** Physisorption of adventitious hydrocarbons onto the H-terminated Si(111) surface can cause the Si–H IR peak to broaden and shift to lower wavenumber, whereas oxidation of the Si–Si back-bonds causes the Si–H peak to shift to slightly higher energy.<sup>19,24,30,31,96,97</sup> To confirm our assignments of the IR peaks that appeared after exposure to  $CD_3OD$  solutions containing  $FcBF_4$ ,  $I_2$ , or  $Br_2$  ( $2070\text{ cm}^{-1}$  ( $\nu_s(CD_3)$ ) and  $2225\text{ cm}^{-1}$  ( $\nu_{as}(CD_3)$ )), experiments were performed using  $CH_3OH$  as the solvent.

Exposure to  $CH_3OH$  or to  $Fc-CH_3OH$  produced some broadening of the Si–H IR peak but resulted in no dramatic reductions in IR peak intensity. Exposure of the monohydride-terminated Si(111) ATR crystals to  $CH_3OH-Fc^+$ ,  $CH_3OH-I_2$ , or  $CH_3OH-Br_2$  solutions eliminated the Si–H peak at  $2083\text{ cm}^{-1}$ , but no peaks were observed at  $2070$  or  $2225\text{ cm}^{-1}$  (see Supporting Information). Because a large amount of adventitious hydrocarbon was present on the oxidized ATR crystals used to collect the background spectra, large negative peaks were present in the C–H region of spectra that used the oxidized crystal as the background. However, little adventitious hydrocarbon was present on crystals that had been freshly etched with 40%  $NH_4F(aq)$ , and spectra that were collected using such freshly etched crystals as the background showed that new IR peaks appeared at  $2840\text{ cm}^{-1}$  ( $\nu_s(CH_3)$ ) and  $2960\text{ cm}^{-1}$  ( $\nu_{as}(CH_3)$ ) after exposure to the  $CH_3OH$  solutions. These peak positions closely match the peak positions established for the symmetric and asymmetric

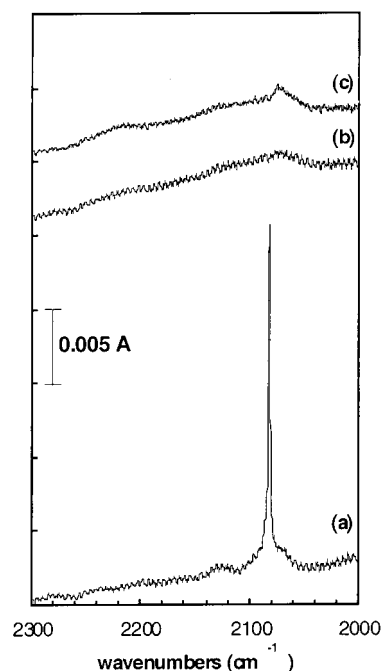


**Figure 4.** FT-IR spectra of a Si(111) ATR crystal after (a) etching in  $N_2$ -sparged 40%  $NH_4F(aq)$ , (b) immersion for 5 min in a  $CH_3OH$  solution containing 200 mM  $FcBF_4$  and then washing with  $CD_3OD$ , and (c) immersion for 5 h in  $CD_3OD$ .

methyl stretches of gas-phase  $CH_3OH$  ( $\nu_s(CH_3)$  at  $2844\text{ cm}^{-1}$  and  $\nu_{as}(CH_3)$  at  $2960\text{ cm}^{-1}$ ),<sup>94</sup> as expected for a Si– $OCH_3$  species. These peaks were not observed after exposure of monohydride-terminated Si(111) ATR crystals to the  $CD_3OD$  solutions. In addition, exposure of  $HF(aq)$ -etched Si(100) surfaces to  $FcBF_4$ ,  $I_2$ , or  $Br_2$  in  $CD_3OD$  solutions (vide infra) produced a peak at  $2070\text{ cm}^{-1}$  that was essentially identical in shape to the one observed at  $2070\text{ cm}^{-1}$  on the Si(111) surface of Figure 1d, and this peak is significantly narrower than the Si– $H_x$  peak that is observed on the freshly prepared H-terminated Si(100) surface. Thus, the assignment of the peaks at  $2070$  and  $2225\text{ cm}^{-1}$  as arising from surficial Si– $OCD_3$  groups appears to be robust.

**3. Persistence of F, I, and Br on the Surface and Exchangeability of the  $-OCH_3$  Groups.** Figure 4 shows the IR spectral changes that occurred in the  $2000\text{--}2300\text{ cm}^{-1}$  region for a Si(111) ATR crystal following washing of the  $-OCH_3$ -terminated surface (obtained from exposure to 200 mM  $FcBF_4$  in  $CH_3OH$ ) with  $CD_3OD$  and after immersing the  $-OCH_3$ -terminated crystal in  $CD_3OD$  for 5 h. The sharp silicon monohydride peak at  $2083\text{ cm}^{-1}$  present on the freshly 40%  $NH_4F(aq)$ -etched ATR crystal (Figure 4a) was completely eliminated after a 5 min exposure of the sample to a  $CH_3OH$  solution of  $FcBF_4$ , followed by washing with  $CD_3OD$  (Figure 4b). As is apparent from the figure, washing with  $CD_3OD$  did not produce significant peaks at  $2070$  or  $2225\text{ cm}^{-1}$ , indicating that on the time scale of exposure to  $CD_3OD$  during washing no detectable substitution of surficial  $-OCH_3$  or of the surficial F-containing species with  $-OCD_3$  had occurred. Analogous experiments performed by immersing a freshly etched Si(111) ATR crystal into  $CH_3OH$  solutions of  $I_2$  or  $Br_2$ , followed by washing with  $CD_3OD$ , produced similar spectra with elimination of the silicon monohydride peak at  $2083\text{ cm}^{-1}$  and the growth of no, or very small, peaks at  $2070$  and  $2225\text{ cm}^{-1}$ . Similarly, immersing freshly etched Si(111) ATR crystals into  $CD_3OD$  solutions containing  $FcBF_4$ ,  $I_2$ , or  $Br_2$  followed by washing with  $CH_3OH$  resulted in complete elimination of the monohydride peak at  $2083\text{ cm}^{-1}$

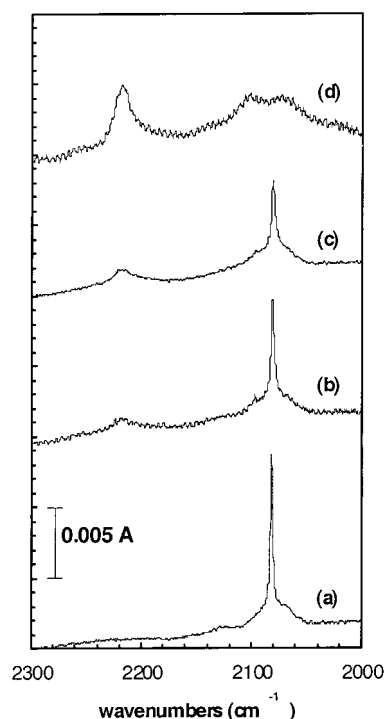


**Figure 5.** FT-IR spectra of a Si(111) ATR crystal after (a) etching in  $\text{N}_2$ -sparged 40%  $\text{NH}_4\text{F}(\text{aq})$ , (b) immersion for 5 min in  $\text{C}_4\text{D}_9\text{OD}$ , (c) immersion for 3–5 min in  $\text{C}_4\text{D}_9\text{OD}$  containing 200 mM ferrocene, and (d) subsequent immersion for 3–5 min in  $\text{C}_4\text{D}_9\text{OD}$  containing 200 mM ferrocenium  $[\text{Fc}^+]$ .

and growth of the  $\text{CD}_3$  peaks at 2070 and 2225  $\text{cm}^{-1}$ , identical to the spectra obtained from surfaces treated as described in section 1 above. The XP spectra obtained from these surfaces did not differ significantly from those described in sections 1 and 2.

As seen in Figure 4c, immersing the  $-\text{OCH}_3$ -terminated surface into  $\text{CD}_3\text{OD}$  for 5 h did result in significant growth of the  $-\text{CD}_3$  peaks at 2070 and 2225  $\text{cm}^{-1}$ . The size of the F peak in the XP survey spectrum and of the oxidized Si peak in the high-resolution Si 2p XP spectrum did not change after immersion in  $\text{CD}_3\text{OD}$  for 5 h. Thus, on this longer time scale the  $-\text{OD}_3$  groups must have exchanged with the  $-\text{OCH}_3$  groups on the surface, not by replacing the F-containing surface species. The retention of strongly bound F-containing groups after immersion for 5 h in  $\text{CD}_3\text{OD}$ , concomitant with substantial  $-\text{OCD}_3$  formation, indicates the formation of the  $-\text{OCH}_3$ -terminated surface and subsequent substitution with  $-\text{OCD}_3$  groups does not proceed by dissolution of the Si surface.

**4. Exposure to  $\text{C}_4\text{D}_9\text{OD}$ .** Derivatization experiments were also performed in  $\text{C}_4\text{D}_9\text{OD}$  and  $\text{C}_4\text{H}_9\text{OH}$  solutions. Because  $\text{FcBF}_4$  is substantially less soluble in butanol than methanol, the exposure times were increased relative to the times used in the methanol experiments. Immersing a Si sample in  $\text{C}_4\text{D}_9\text{OD}$  for 5 min (Figure 5b) followed by subsequent immersion in saturated  $\text{C}_4\text{D}_9\text{OD}-\text{Fc}$  for 5 min (Figure 5c) produced some broadening of the Si-H IR peak at 2083  $\text{cm}^{-1}$  and some loss in intensity of this signal. However, immersion of the H-terminated Si(111) into  $\text{C}_4\text{D}_9\text{OD}$  saturated with  $\text{FcBF}_4$  produced much more significant changes in the IR spectra of the sample, with a complete loss of the sharp positive peak near 2083  $\text{cm}^{-1}$  (Figure 5d) and production of negative peaks in the C-H region of the difference spectrum. The relatively sharp peak at 2220  $\text{cm}^{-1}$ , assigned to the C-D stretch, was quite apparent, and the peak at 2073  $\text{cm}^{-1}$  also increased but to a lesser extent. An additional peak at 2120  $\text{cm}^{-1}$  also was observed, perhaps arising

from the stretching of Si-H groups bonded to neighboring Si- $\text{OC}_4\text{D}_9$  groups.

The high-resolution XP scans of the Si 2p region showed a slight rise in the baseline in the region at a binding energy where the oxidized silicon peak would likely appear, but less signal intensity was apparent in this region than was observed when the H-terminated Si surface was exposed to oxidizing methanol solutions (Table 2 and Supporting Information). Thus, a lower density of  $-\text{OC}_4\text{H}_9$  groups is present on such surfaces, as expected because of the larger diameter of the  $-\text{OC}_4\text{H}_9$  group relative to the  $-\text{OCH}_3$  group. The survey XP scans indicate that after exposure to  $\text{C}_4\text{H}_9\text{OH}-\text{FcBF}_4$  approximately 15% of a monolayer of F was present on the surface and the hydrocarbon coverage increased to approximately 2.6 monolayers (Table 1). The increase in the O 1s/C 1s peak area ratio is in accord with expectations for formation of a covalently attached surface alkoxyl group in addition to the presence of adventitious adsorbed hydrocarbons.

**5. Exposure to  $\text{C}_4\text{H}_9\text{OH}$ .** The assignments of the C-D stretches in the IR spectra presented above were confirmed by experiments in which  $\text{C}_4\text{H}_9\text{OH}$  was used as the solvent. Exposure of the 40%  $\text{NH}_4\text{F}(\text{aq})$ -etched Si(111) ATR crystal to  $\text{C}_4\text{H}_9\text{OH}$  or to  $\text{C}_4\text{H}_9\text{OH}-\text{Fc}$  produced minimal changes in the IR spectra; however, exposure to  $\text{C}_4\text{H}_9\text{OH}-\text{FcBF}_4$  completely eliminated the sharp peak at 2083  $\text{cm}^{-1}$ , leaving a broad peak centered at 2080  $\text{cm}^{-1}$  (see Supporting Information). The peaks at 2220 and 2073  $\text{cm}^{-1}$  (that were assigned above to C-D stretches) did not appear, while peaks were instead apparent in the C-H region. The XP spectra were identical to those obtained from the surfaces treated analogously but with  $\text{C}_4\text{D}_9\text{OD}$  instead of  $\text{C}_4\text{H}_9\text{OH}$  as the solvent.

**6. Exposure to  $\text{HO}(\text{CH}_2)_3\text{CF}_3$ .** Although the presence of C-D vibrational stretches after exposure to  $\text{Fc}^+$  solutions of deuterated alcohols provides convincing evidence of the attachment of the alcohol to the Si surface, experiments were performed using a fluorine-tagged alcohol,  $\text{HO}(\text{CH}_2)_3\text{CF}_3$ , in an effort to quantify the extent of surface modification. This alcohol was chosen because F has a large XPS cross section that should enable quantification of the surface coverage.<sup>78</sup> The presence of F in the alcohol should allow corroboration of the surface coverage through calculation of the F/Si ratio, the fluorinated C/Si ratio, and the oxidized to unoxidized Si ratio. In addition, because the C-F bonds are separated from the C-O bond by three  $\text{CH}_2$  groups, preparation of the corresponding lithium alkoxide was possible. Finally, a surface containing Si- $\text{O}(\text{CH}_2)_3\text{CF}_3$  groups could also be independently prepared by a two-step chlorination/alkoxylation procedure (vide infra).

Figure 6 shows the surface IR spectra of a (111)-oriented Si ATR crystal, relative to that of the oxidized Si surface, after the crystal had been etched and exposed to  $\text{HO}(\text{CH}_2)_3\text{CF}_3$ ,  $\text{HO}(\text{CH}_2)_3\text{CF}_3-\text{Fc}$ , and  $\text{HO}(\text{CH}_2)_3\text{CF}_3-\text{FcBF}_4$  solutions. As with the methanol and butanol experiments, exposure of the monohydride-terminated Si(111) ATR crystal to the neat alcohol and to the alcoholic Fc solution produced only minor reductions in the Si-H peak intensity (Figure 6, spectra b and c). Moreover, no changes were discernible in the survey (Table 1) and Si 2p high-resolution (Table 2) XP spectra after exposure to these solutions, including no significant growth of the F peak.

As with the methanol and butanol solutions, immersion of the Si(111) crystal into saturated  $\text{HO}(\text{CH}_2)_3\text{CF}_3-\text{FcBF}_4$  produced significant changes in both the IR (Figure 6d) and XP spectra of the sample (Tables 1 and 2 and Supporting Information). The sharp monohydride peak in the IR spectrum was eliminated, leaving a broad peak centered at 2080  $\text{cm}^{-1}$ . The

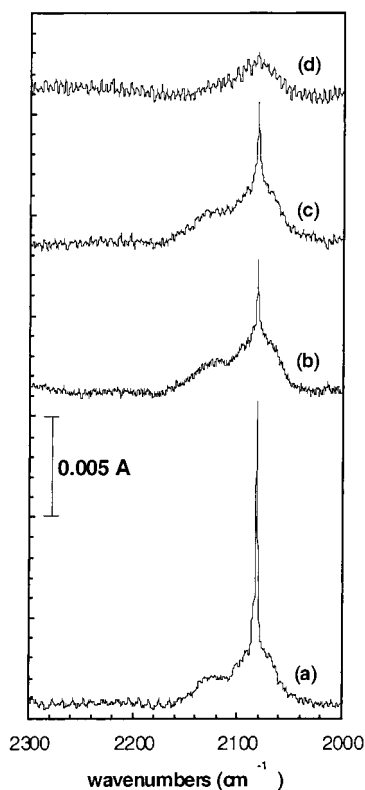


**Figure 6.** FT-IR spectra of a Si(111) ATR crystal after (a) etching in  $\text{N}_2$ -sparged 40%  $\text{NH}_4\text{F}(\text{aq})$ , (b) immersion for 5 min in  $\text{HO}(\text{CH}_2)_3\text{CF}_3$ , (c) immersion for 3–5 min in  $\text{HO}(\text{CH}_2)_3\text{CF}_3$  containing 200 mM ferrocene, and (d) immersion for 3–5 min in  $\text{HO}(\text{CH}_2)_3\text{CF}_3$  containing 200 mM ferrocenium  $[\text{BF}_4]$ .

XP survey spectra (Table 1) showed small signals indicative of oxidized Si, with the O 1s/Si 2p peak ratio in the survey scan increasing from 0.20 to 0.43. The O 1s/C 1s peak area ratio did not decrease significantly from 1:1, as would have been expected on the basis of the 1:4 ratio of O/C in the alcohol. The F 1s intensity increased significantly only after immersion into the  $\text{HO}(\text{CH}_2)_3\text{CF}_3\text{--FcBF}_4$  solution, to about 75% of a monolayer of F (Table 1), which would correspond to 25% of a monolayer of  $\text{--CF}_3$ , which is reasonably close to the 33% of a monolayer of  $\text{--CF}_3$  groups that would be expected for the highest possible packing of  $\text{--CF}_3$  groups onto the surface. Furthermore, a signal from fluorinated C was also observed. The high-resolution scans of the Si 2p region showed an oxidized Si 2p peak corresponding to approximately 20% of a monolayer (Table 2), in reasonable agreement with the 25% coverage calculated from the intensity of the F 1s XPS signal.

**7. Chlorination Followed by Reaction with Lithium Alkoxide.** Methoxylated surfaces were prepared by an independent method to facilitate comparison of the spectra of these surfaces to those obtained by immersion of H-terminated Si into  $\text{CD}_3\text{OD--FcBF}_4$  solutions. A variation of a two-step, chlorination/alkylation procedure,<sup>1</sup> in which the chlorinated surface was reacted with  $\text{LiOCH}_3$  or  $\text{LiOCD}_3$ , was used for this purpose.

Immersion of a Si ATR crystal in  $\text{C}_6\text{H}_5\text{Cl--PCl}_5$  followed by reaction with  $\text{LiOCH}_3$  completely eliminated the sharp silicon monohydride IR peak, leaving a small, broad peak in the same region, and no peaks appeared at  $2070\text{ cm}^{-1}$  ( $\nu_s(\text{CD}_3)$ ) and  $2225\text{ cm}^{-1}$  ( $\nu_{as}(\text{CD}_3)$ ) (see Supporting Information). When the chlorinated Si surface was exposed to  $\text{LiOCD}_3$ , two peaks associated with the  $\nu_s(\text{CD}_3)$  and  $\nu_{as}(\text{CD}_3)$  stretches appeared at  $2070$  and  $2220\text{ cm}^{-1}$ , respectively (Figure 7). This spectrum is very similar to the spectrum obtained after exposure of (111)-

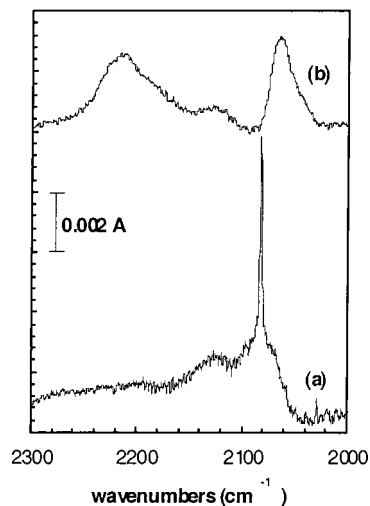


**Figure 7.** FT-IR spectra of a Si(111) ATR crystal after (a) etching in  $\text{N}_2$ -sparged 40%  $\text{NH}_4\text{F}(\text{aq})$  and (b) immersion in a saturated  $\text{C}_6\text{H}_5\text{Cl}$  solution of  $\text{PCl}_5$  at  $90^\circ\text{C}$  for 50 min followed by reaction of the chlorinated surface in  $\text{CD}_3\text{OD}$  containing 1 M  $\text{LiOCD}_3$  at  $70^\circ\text{C}$  for 19 h.

oriented Si to  $\text{CD}_3\text{OD--FcBF}_4$ ,  $\text{CD}_3\text{OD--I}_2$ , or  $\text{CD}_3\text{OD--Br}_2$  (Figure 1).

The results of the two-step procedure were similar when  $\text{LiO}(\text{CH}_2)_3\text{CF}_3\text{--THF}$  solutions were used. Notably, the Cl peaks in the XPS survey scan were reduced in intensity by  $\sim 30\%$  but were not completely eliminated after exposure to  $\text{LiO}(\text{CH}_2)_3\text{CF}_3\text{--THF}$  (Tables 1 and 2). The Si 2p high-resolution spectra (Table 2) show that less than a monolayer of oxidized Si was present after the two-step chlorination/alkoxylation procedure using the F-tagged lithium butoxide. The observed decrease in the extent of reaction with the trifluorobutanol reagent, as evidenced by incomplete reaction of the Cl on the surface, may result from a combination of its longer chain length and the greater size of the  $\text{--CF}_3$  tail inhibiting close packing of the monolayer or may occur because the reaction was performed in THF rather than in the parent alcohol, which reduced the solubility of the alkoxide. The hydrocarbon coverage increased noticeably, to approximately 4.9 monolayers (Table 1), as would be expected for alkoxylation with a  $\text{C}_4$  functionality. However, the amount of adventitious hydrocarbon will depend on the surface energy, which could be changed significantly in the presence of  $\text{--CF}_3$  headgroups.

**B. Si(100) Surface Chemistry.** The Si(100) surface was observed generally to react similarly to the Si(111) surface. The IR data on the Si(100) surface orientation are useful to confirm the peak assignments advanced above for the Si(111) surface. The remainder of the comments focus on other differences in the reactivity observed for the (100) and (111) surface orientations.

**1. Exposure to  $\text{CD}_3\text{OD}$ .** Etching a (100)-oriented Si crystal in 48%  $\text{HF}(\text{aq})$  is known to produce a mixture of mono-, di-, and trihydride species on the surface;<sup>98</sup> thus, a relatively broad peak centered at  $\sim 2100\text{ cm}^{-1}$  was observed in the IR spectra of the freshly etched crystal (Figure 8a). Immersing the etched crystal in  $\text{CD}_3\text{OD}$  for 2 min followed by immersing the crystal in saturated  $\text{CD}_3\text{OD--Fc}$  for 2 min produced only a slight decrease in intensity of the  $\text{SiH}_x$  peak (Figure 8b,c). Two negative-going peaks in the spectra collected against the freshly etched crystal indicated that some of the  $\text{SiH}_x$  species (possibly at strained defect sites) reacted to a small extent. When the crystal was exposed to saturated  $\text{CD}_3\text{OD--FcBF}_4$  for 2 min, several major changes were observed in the IR spectrum (Figure

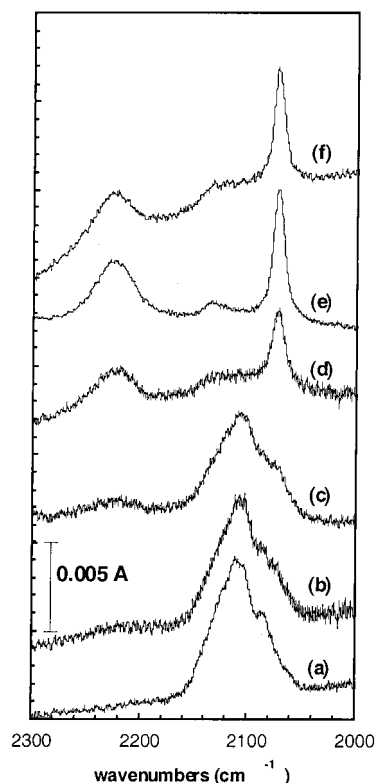


**Figure 8.** FT-IR spectra of a Si(100) ATR crystal after (a) etching in  $N_2$ -sparged 48% HF(aq), (b) immersion for 5 min in  $CD_3OD$ , (c) immersion for 3–5 min in  $CD_3OD$  containing 200 mM ferrocene, and (d) immersion for 3–5 min in  $CD_3OD$  containing 200 mM ferrocenium  $[BF_4]$  and (e) a different H-terminated ATR crystal after immersion for 15 min in  $CD_3OD$  containing 25 mM  $I_2$  and (f) a different H-terminated ATR crystal after immersion for 15 min in  $CD_3OD$  containing 200 mM  $Br_2$ .

8d). First, the  $SiH_x$  peak was greatly reduced in intensity. Second, a new, sharper peak appeared at  $2073\text{ cm}^{-1}$ , and a broad peak, centered at  $2225\text{ cm}^{-1}$ , appeared. These peaks have been assigned above as  $\nu_s(CD_3)$  and  $\nu_{as}(CD_3)$ , respectively. No positive peaks in the C–H stretching region appeared in the difference spectrum relative to the freshly etched surface, in fact the presence of negative peaks in the region suggest that the  $-CD_3$  groups replaced some adventitious hydrocarbon present on the freshly etched crystal that was used as the background. These spectral changes are consistent with those observed after immersion of (111)-oriented Si into  $CD_3OD$ – $FcBF_4$ ,  $CD_3OD$ – $I_2$ , and  $CD_3OD$ – $Br_2$  solutions (Figure 1) and after the two-step chlorination/ $LiOCD_3$  reaction sequence (Figure 7).

Similar IR spectral changes were observed after immersing a hydrogen-terminated Si ATR crystal for 15 min in  $CD_3OD$  solutions that contained either 25 mM  $I_2$  (Figure 8e) or 200 mM  $Br_2$  (Figure 8f). However, in contrast to the behavior of Si(111) surfaces, the intensities of the C–D peaks produced after exposure of the H-terminated Si(100) surface to  $CD_3OD$  solutions containing  $I_2$  or  $Br_2$  were larger than the peak intensities produced after exposure to the methanolic  $FcBF_4$  solution.

The survey scan XP spectra collected on Si(100) surfaces exposed to  $I_2$ – $CD_3OD$  and  $Br_2$ – $CD_3OD$  surfaces were similar to those observed for the  $FcBF_4$ – $CD_3OD$  exposed surfaces (Tables 3 and 4). The size of the O and C peaks increased to the same extent, and the O/C ratio increased from 2:3 to 3:1, indicating that a hydrocarbon overlayer of similar composition and quantity was formed in each case. Based on the C 1s/Si 2p

peak area ratio, the hydrocarbon coverage did not change appreciably after exposure to the different treatments (approximately 2.5–2.9 monolayers) even though the oxygen-to-carbon ratio increased noticeably. This is consistent with the replacement of the adventitious hydrocarbons that have a relatively low oxygen content by methoxy groups that have an O/C stoichiometric ratio of 1:1. The oxidized Si peak observed in the Si 2p region (Figure 9) was similar in size, shape, and position to that obtained after exposure of Si(100) surfaces to methanolic  $FcBF_4$  solutions, suggesting that a similar overlayer species and coverage was obtained after the methanolic  $FcBF_4$ ,  $I_2$ , or  $Br_2$  treatments. However, the surfaces produced by these various treatments are not identical. The surface exposed to  $FcBF_4$ –methanol exhibited a F peak (corresponding to approximately 20% of a monolayer of F), the surface exposed to  $I_2$ –methanol exhibited an I peak (corresponding to approximately 13% of a monolayer of I), and the surface exposed to  $Br_2$ –methanol exhibited a Br peak (corresponding to approximately 29% of a monolayer of Br) (Tables 3 and 4).

The Si(100) surfaces exhibited larger  $\nu_s(CD_3)$  and  $\nu_{as}(CD_3)$  peaks in the IR spectra but smaller F, I, or Br XPS peak intensities than those that were observed for analogously treated Si(111) surfaces. The larger fractional coverage of  $-OCD_3$  groups and the smaller halogen coverage on the (100) surface may result from the greater steric interactions between halogen atoms on neighboring sites on the Si(100) surface or from a greater inherent reactivity of the surface due to the angle of bond inclination from the surface or a larger fraction of defect sites on the 48% HF(aq)-etched Si(100) surfaces than that on the 40%  $NH_4F$ (aq)-etched Si(111) surfaces.

**2. Exposure to  $CH_3OH$ .** Additional support for the  $-CD_3$  peak assignments ( $2070\text{ cm}^{-1}$  ( $\nu_s(CD_3)$ ) and  $2225\text{ cm}^{-1}$  ( $\nu_{as}(CD_3)$ )) was obtained by exposing the hydrogen-terminated Si(100) surface to  $CH_3OH$  solutions (see Supporting Information). Exposing the ATR crystals to  $CH_3OH$  and  $Fc$ – $CH_3OH$  solutions produced only a slight decrease in intensity of the  $SiH_x$  peak. Immersing the crystal into saturated  $FcBF_4$ – $CH_3OH$  for 2 min,  $CH_3OH$ – $I_2$  for 15 min, or  $CH_3OH$ – $Br_2$  for 15 min greatly reduced the  $Si$ – $H_x$  peak intensity and produced relatively strong positive peaks in the C–H region in the difference spectra of the treated crystal. No peaks appeared at  $2070$  or  $2225\text{ cm}^{-1}$ . The changes in the XP spectra were identical to those observed after immersion in  $CD_3OD$  solutions.

**3. Persistence of F, I, and Br on the Surface and Exchangeability of the  $-OCH_3$  Groups.** Figure 10 shows the IR spectral changes that occurred in the  $2000$ – $2300\text{ cm}^{-1}$  region for a Si(100) ATR crystal following washing of the  $-OCH_3$ -terminated surface with  $CD_3OD$  and after immersing the  $-OCH_3$ -terminated crystal in  $CD_3OD$  for 2 h. The broad silicon hydride peak present on the freshly 48% HF(aq)-etched ATR crystal (Figure 10a) was almost completely eliminated after exposure to a  $CH_3OH$  solution of  $FcBF_4$  for 5 min, followed by washing with  $CD_3OD$  (Figure 10b). As is apparent from the figure, washing with  $CD_3OD$  produced significant peaks at  $2070$  and  $2225\text{ cm}^{-1}$  (in contrast to the Si(111) surface, vide supra), indicating that on the time scale of exposure to  $CD_3OD$  during washing, substitution with  $-OCD_3$  of surficial  $-OCH_3$  or of the surficial F-containing species occurred on the Si(100) surface. The XP spectra obtained from these surfaces did not differ significantly from those described in sections B.1 and B.2 and are included in the averages given in Tables 3 and 4. As seen in Figure 10c, immersing the  $-OCH_3$ -terminated surface into  $CD_3OD$  for 2 h did not result in significant further growth of the  $-CD_3$  peaks at  $2070$  and  $2225\text{ cm}^{-1}$ . The size of

**TABLE 3: Ratio of XPS Raw Peak Intensities for Si(100) Surfaces and Calculated Monolayer Coverages**

reaction	Si 2s/Si 2p	C 1s/Si 2p	O 1s/Si 2p	O 1s/C 1s	F 1s/Si 2p	I 4d/Si 2p	I 3d <sub>5/2</sub> /Si 2p	I 3d <sub>3/2</sub> /Si 2p	Br 3d <sub>3/2</sub> /Si 2p	Cl 2s/Si 2p
48% HF	1.21 ± 0.04	0.45 ± 0.10	0.32 ± 0.11	0.72 ± 0.16	0.05 ± 0.05					
CH <sub>3</sub> OH–FeBF <sub>4</sub>	1.22 ± 0.03	0.40 ± 0.08	0.96 ± 0.10	2.42 ± 0.39	0.20 ± 0.04					
CH <sub>3</sub> OH–I <sub>2</sub> (8 mM)	1.22 ± 0.05	0.38 ± 0.03	0.90 ± 0.04	2.36 ± 0.10	0.05 ± 0.04	0.06 ± 0.02	0.29 ± 0.03	0.24 ± 0.07		
CH <sub>3</sub> OH–I <sub>2</sub> (63 mM)	1.20 ± 0.03	0.35 ± 0.03	1.16 ± 0.02	3.28 ± 0.23		0.05 ± 0.01	0.28 ± 0.02	0.22 ± 0.02		
CH <sub>3</sub> OH–Br <sub>2</sub>	1.24 ± 0.03	0.42 ± 0.04	1.21 ± 0.08	2.92 ± 0.09	0.07 ± 0.01				0.114 ± 0.003	
C <sub>6</sub> H <sub>5</sub> Cl–PCl <sub>5</sub>	1.20 ± 0.02	0.28 ± 0.08	0.34 ± 0.26	0.96 ± 0.08	0.01 ± 0.02					0.23 ± 0.02
Si–Cl + LiOCH <sub>3</sub>	1.20 ± 0.02	0.26 ± 0.06	0.43 ± 0.19	0.59 ± 0.43						0.01 ± 0.03

reaction	monolayers hydrocarbon (from C 1s/Si 2p) <sup>a</sup>	equivalent monolayers <sup>b</sup> O (from O 1s/Si 2p) <sup>b</sup>	monolayers <sup>c</sup> F (from F 1s/Si 2p) <sup>b</sup>	monolayers <sup>c</sup> I (from I 4d/Si 2p) <sup>b</sup>	monolayers <sup>c</sup> Br (from Br 3d <sub>3/2</sub> /Si 2p) <sup>b</sup>	monolayers <sup>c</sup> Cl (from Cl 2s/Si 2p) <sup>b</sup>
48% HF	2.9	0.79	0.057			
CH <sub>3</sub> OH–FeBF <sub>4</sub>	2.7	1.9	0.22			
CH <sub>3</sub> OH–I <sub>2</sub> (8 mM)	2.6	1.8	0.057	0.13		
CH <sub>3</sub> OH–I <sub>2</sub> (63 mM)	2.5	2.2		0.11		
CH <sub>3</sub> OH–Br <sub>2</sub>	2.8	2.3	0.080		0.29	
C <sub>6</sub> H <sub>5</sub> Cl–PCl <sub>5</sub>	2.4	0.89	0.011			0.77
Si–Cl + LiOCH <sub>3</sub>	1.9	1.0				0.037

<sup>a</sup> Calculated using eq 3,<sup>78</sup> where the sensitivity factors were 1.00 for C 1s and 0.90 for Si 2p, the escape depth of the Si 2p electron through the hydrocarbon overlayer was taken to be 3.5 nm,<sup>81,82</sup> the molar density of Si is  $8.30 \times 10^{-2} \text{ mol cm}^{-3}$ , the molar density of the overlayer was estimated to be  $3.3 \times 10^{-2} \text{ mol cm}^{-3}$ ,<sup>81</sup> and the thickness of a monolayer was taken to be 0.48 nm.<sup>81</sup> <sup>b</sup> Monolayer coverages  $\geq 1.0$  were calculated using eq 3 and monolayer coverages  $< 1.0$  were calculated using eq 5.<sup>78</sup> The sensitivity factors were 2.52 for O 1s and 0.90 for Si 2p,<sup>78,79</sup> the escape depth of the Si 2p electron through the overlayer was taken to be 2.6 nm,<sup>78</sup> the atomic density of Si is  $5.0 \times 10^{22} \text{ atoms cm}^{-3}$ , the atomic density of O is  $3.46 \times 10^{22} \text{ atoms cm}^{-3}$ ,<sup>80</sup> and the thickness of a monolayer ( $d_{ov}$  in eq 3 and  $a_{ov}$  in eq 5) is estimated as 0.31 nm.<sup>78</sup> <sup>c</sup> Monolayer coverages were calculated using eq 5,<sup>78</sup> where the sensitivity factors were 3.40 for F 1s, 1.70 for Cl 2s, 2.84 for Br 3d, 4.69 for I 4d, and 0.90 for Si 2p,<sup>78,79</sup> the escape depth of the Si 2p photoelectrons through the overlayer was taken to be 2.1, 2.6, 2.7, 2.7, and 3.2 nm for F, Cl, Br, and I, respectively,<sup>78</sup> the atomic densities (atoms  $\text{cm}^{-3}$ ) were F =  $5.28 \times 10^{22}$ , Cl =  $3.43 \times 10^{22}$ , Br =  $3.04 \times 10^{22}$ , I =  $2.34 \times 10^{22}$ , and Si =  $5.0 \times 10^{22}$ ,<sup>80</sup> and the atomic diameter of the atoms forming the overlayer was estimated to be 0.26, 0.31, 0.32, and 0.35 nm for F, Cl, Br, and I, respectively.<sup>78</sup>

**TABLE 4: Coverage of Oxidized Si from High-Resolution XPS of Si(100)**

reaction	SiO <sub>x</sub> 2p/Si <sub>bulk</sub> 2p	% monolayer <sup>a</sup> SiO <sub>x</sub>	% monolayer <sup>b</sup> Si <sup>1+</sup>
48% HF etched	0	0	0
CH <sub>3</sub> OH–FeBF <sub>4</sub>	0.062 ± 0.008	34 ± 4	34 ± 4
CH <sub>3</sub> OH–I <sub>2</sub> (8 mM)	0.050 ± 0.002	27 ± 1	28 ± 1
CH <sub>3</sub> OH–I <sub>2</sub> (63 mM)	0.098 ± 0.002	51 ± 2	54 ± 1
CH <sub>3</sub> OH–Br <sub>2</sub> (200 mM)	0.099 ± 0.003	52 ± 2	55 ± 2
C <sub>6</sub> H <sub>5</sub> Cl–PCl <sub>5</sub>	0.075 ± 0.025	39 ± 12	42 ± 14
Si–Cl + LiOCH <sub>3</sub>	0.011 ± 0.006	5.0 ± 1.5	6.1 ± 1.2

<sup>a</sup> Calculated using eq 8, where the escape depth of the Si 2p electron through an oxide overlayer was taken to be 2.6 nm,<sup>84</sup>  $\theta = 35^\circ$ , the peak ratio of pure Si to pure SiO<sub>2</sub> ( $I_{Si}^0/I_{Ov}^0$ ) in the Si 2p region was determined to be 1.3,<sup>83</sup> and the thickness of a monolayer of SiO<sub>2</sub> was estimated to be 0.35 nm.<sup>83</sup> <sup>b</sup> Calculated using eq 11, in which 18% of the total unattenuated photoelectrons are calculated to originate from the surface atoms ( $6.9 \times 10^{14} \text{ atoms cm}^{-2}$ ) on Si(100). The ratio of the Si 2p peak arising from oxidized Si to the Si 2p peak arising from bulk Si was divided by 0.18 to determine the fraction of surficial Si atoms in an oxidized state.

the F peak in the XP survey spectra and of the oxidized Si peak in the high-resolution Si 2p spectra did not change after immersion for 2 h. Thus, a limited amount of methoxide exchange occurs more rapidly on the Si(100) surface than on the Si(111) surface.

**4. Chlorination Followed by Reaction with Lithium Alkoxide.** The two-step chlorination/methoxylation of Si(100)-oriented crystals using LiOCD<sub>3</sub> or LiOCH<sub>3</sub> produced a 66% reduction in the Si–H<sub>x</sub> peak intensity. When the chlorinated surface was reacted with LiOCH<sub>3</sub>, no peaks attributable to  $\nu_s(\text{CD}_3)$  and  $\nu_{as}(\text{CD}_3)$  appeared (see Supporting Information), while small peaks appeared in the C–H region of the difference spectrum,

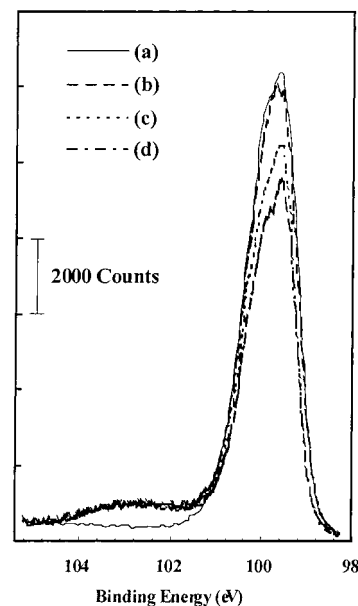


**Figure 9.** High-resolution Si 2p XP spectra of a Si(100) ATR crystal after (a) etching in N<sub>2</sub>-sparged 48% HF(aq) and (b) immersion for 5 min in CD<sub>3</sub>OD, for 3–5 min in CD<sub>3</sub>OD containing 200 mM ferrocene, and then for 3–5 min in CD<sub>3</sub>OD containing 200 mM ferrocenium [BF<sub>4</sub>]<sup>–</sup> and (c) a different H-terminated ATR crystal after immersion for 15 min in CD<sub>3</sub>OD containing 25 mM I<sub>2</sub> and (d) a different H-terminated ATR crystal after immersion for 15 min in CD<sub>3</sub>OD containing 200 mM Br<sub>2</sub>.

indicating an increase in the amount of hydrocarbon on the surface. The analogous two-step process using LiOCD<sub>3</sub> also resulted in a reduction in the intensity of the IR Si–H peak (Figure 11). Peaks arising from  $\nu_s(\text{CD}_3)$  and  $\nu_{as}(\text{CD}_3)$  grew in at 2070  $\text{cm}^{-1}$  and at 2220  $\text{cm}^{-1}$ , indicative of the presence of surficial –OCD<sub>3</sub> groups. Negative peaks appeared in the C–H region in the difference spectra under such conditions.

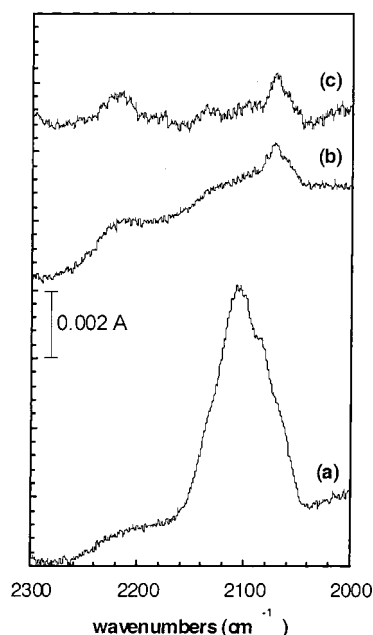


**Figure 10.** FT-IR spectra of a Si(100) ATR crystal after (a) etching in  $N_2$ -sparged 48% HF(aq), (b) immersion for 5 min in a  $CH_3OH$  solution containing  $FcBF_4$  and then washing with  $CD_3OD$ , and (c) immersion for 2 h in  $CD_3OD$ .

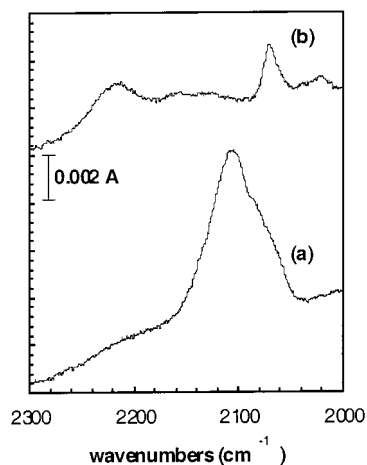


**Figure 11.** FT-IR spectra of a Si(100) ATR crystal after (a) etching in  $N_2$ -sparged 48% HF(aq) and (b) immersion in a saturated  $C_6H_5Cl$  solution of  $PCl_5$  at 90 °C for 50 min followed by reaction of the chlorinated surface in  $CD_3OD$  containing 1.0 M  $LiOCD_3$  at 70 °C for 24 h.

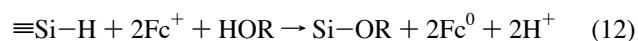
In the XP survey spectra, the O/C ratio increased from 2:3 to 1:1 upon chlorination and then increased to 2:1 after alkoxylation (vs 3:1 after immersing the H-terminated Si(100) crystal in methanol containing  $FcBF_4$ ,  $I_2$ , or  $Br_2$ ) (Tables 3 and 4). This smaller increase in the O/C ratio likely results from the larger amount of low-oxygen-fraction adventitious hydrocarbon present on the surface (approximately 3.7 monolayers). The chlorine was completely removed during the reaction with  $LiOCD_3$ . The amount of oxidized Si in the high-resolution scans of the Si 2p region was much less than that observed for Si(100) surfaces that had been exposed to  $CH_3OH$ – $FcBF_4$  treatment (Table 4). The lower surface coverage obtained using the two-step procedure on the Si(100) surfaces is in contrast to the results with the Si(111) surface, for which nominally identical coverages were obtained for the two-step method relative to immersion into methanolic  $FcBF_4$ ,  $I_2$ , or  $Br_2$  solutions. A lower Cl coverage is apparently obtained on Si(100) than on

Si(111) by reaction with  $PCl_5$ – $C_6H_5Cl$ , as can be seen by comparing Tables 1 and 3.

#### IV. Discussion

**A. Oxidative Activation of H-Terminated Si toward Alkoxylation.** The Si surfaces studied in this work clearly formed Si–OR bonds upon exposure to alcoholic solutions that contained mild oxidants. In  $CH_3OH$ ,  $CD_3OD$ ,  $CF_3(CH_2)_3OH$ ,  $C_4H_9OH$ , or  $C_4D_9OD$ , addition of the one-electron oxidant  $Fc^+$  or of the oxidizing species  $I_2$  or  $Br_2$  produced diagnostic changes in the IR spectra that clearly indicated formation of surficial Si–OR groups. Under our reaction conditions, both the presence of a nucleophilic alcohol and the presence of an oxidant were required to produce a detectable surface alkoxylation product. For example, exposure of Si(100) or Si(111) surfaces to saturated solutions of  $FcBF_4$  in THF produced a broadening but no significant reduction in the integrated intensity of the Si–H stretch in the IR spectra.

A balanced chemical reaction that describes the observed surface chemistry is



where Fc is ferrocenium, representing the prototypical one-electron oxidant used in this work.

The reactivity of oxidatively activated H-terminated crystalline Si with nucleophiles is consistent with prior observations of the reactivity of crystalline Si electrodes and of porous Si surfaces either under anodic bias or under illumination.<sup>24,77,99,100</sup> For example, H-terminated Si(111) electrodes<sup>26</sup> and porous Si electrodes have been reported previously to form Si–OCH<sub>3</sub> bonds under anodic oxidation conditions.<sup>77</sup> Similarly, anodically biased, H-terminated, n-type porous Si and crystalline Si(100) electrodes have been observed to undergo light-induced esterification with carboxylic acids.<sup>24</sup> Alkynes also have been reported to participate in anodic “electrografting” onto H-terminated porous Si.<sup>99</sup> The electrode potentials at which these surface reactions proceed are comparable to the redox potentials of the oxidizing solutions used in this work, consistent with the expectations for oxidative activation of surficial Si–H bonds to nucleophilic attack. The observations reported herein are also consistent with the nucleophilic attack of unbiased porous Si surfaces by alkenes and alkynes in the presence of white light.<sup>100</sup> The formal reduction potential of the photogenerated hole formed from band-gap excitation of Si is close to the potential of the Si valence band,<sup>72,93</sup> so formation of an electron–hole pair will produce an oxidant that can initiate the chemical transformation of eq 12 without addition of an applied potential or an external oxidant to the system. A radical-type transformation that involves homolytic cleavage of the surficial Si–H bond would instead be expected to require high-energy UV excitation.<sup>8,9,77,100</sup>

Horrocks and co-workers have reported the formation of silicon alkoxides on both porous and crystalline Si surfaces exposed to alcohol solutions that did not contain deliberately added oxidants.<sup>28–30,101</sup> Other groups have observed thermal alkoxylation of H-terminated porous Si or H-terminated crystalline Si with neat alcohols.<sup>16,25,27</sup> For example, H-terminated crystalline Si(111) was alkoxyated by exposure to neat decanol at 85 °C for 16 h,<sup>16,25</sup> and porous Si was alkoxyated by exposure to neat decanol for 0.5–24 h at 20–90 °C.<sup>27</sup> Our experiments were performed in  $\leq 15$  min at 25 °C using anhydrous alcohols that were stored over molecular sieves in a  $N_2(g)$  atmosphere, and the Si(111) surfaces were carefully etched to produce a sharp

Si-H peak in the IR spectrum, while polished Si(100) crystals were freshly etched in 48% HF(aq). Under these experimental conditions, no detectable reaction of crystalline H-terminated Si(111) or Si(100) surfaces with alcohols was observed without the addition of oxidants to the solution or without the use of anodic electrochemical or photoelectrochemical conditions. Consistently, Zhu and co-workers have reported that reaction of H-terminated crystalline (111)-oriented Si with neat alcohol for  $\geq 14$  h at 40–80 °C produced negligible surface functionalization compared to a two-step procedure that involves chlorination followed by reaction with neat alcohol.<sup>23</sup> Similarly, Chazalviel and co-workers reported no significant reaction between porous Si and methanol in the absence of anodic current.<sup>77</sup> The same reaction chemistry was observed herein, to first order, for (111)-oriented Si surfaces in which the sharp Si-H stretch contained 80% of the total observed intensity in the entire Si-H region of the IR spectrum (cf. Figure 4a) or for samples that had a lower fraction of the total IR intensity in the Si-H stretching region as monohydridic Si-H species (cf. Figure 1a). The differences in reactivity between the various investigations of Si surface chemistry most likely arise from differences in the reaction temperature, the surface roughness, and the surface strain of the Si being studied or in the amount of molecular oxygen dissolved in the alcohol. For example, the number of etch pits in terraces of an otherwise ideally H-terminated crystalline Si(111) surface is a strong function of the dissolved oxygen concentration.<sup>51</sup> In addition, the reactivity of porous Si may not serve as a robust model for the reactivity of crystalline (111)-oriented Si, as evidenced by the observation that only a fraction of the Si-H sites on porous Si surfaces are generally observed to participate in many chemical transformations.<sup>31–34</sup>

**B. Comparison between the Reaction Chemistry of  $\text{Fc}^+$ ,  $\text{I}_2$ , and  $\text{Br}_2$  Solutions with Crystalline Si(111) and Si(100) Surfaces.** Prior work has generally ascribed the surface chemistry of Si exposed to methanolic or ethanolic solutions of  $\text{Br}_2$  or  $\text{I}_2$  to formation of Si-X ( $\text{X} = \text{I}, \text{Br}$ ) bonding.<sup>42–44</sup> Reflection high-energy electron diffraction data of H-terminated Si(111) after immersion in 0.01 M  $\text{CH}_3\text{OH}-\text{I}_2$  solution only show a  $1 \times 1$  superstructure,<sup>92,102</sup> and such data thus are not conclusive as to the formation of an overlayer under these conditions. Adsorption of I onto the Si(111)  $7 \times 7$  surface under UHV conditions produces a small coherent fraction (0.18 monolayer) of I bound covalently to the atop position of the unreconstructed surface.<sup>16</sup> Similarly, X-ray standing wave (XSW) data on H-terminated crystalline Si(111) surfaces after immersion into  $\text{CH}_3\text{OH}-\text{Br}_2$  solutions indicate that a small coherent fraction ( $<0.3$  monolayer) of covalently bound Br atoms are located above Si atop sites.<sup>52–56</sup> Furthermore, ion-channeling experiments with a total Br coverage of 34% of a monolayer have demonstrated that 80% of the Br atoms lie at the intersection of the (110) and (111) planes, thereby locating them at 2.35 Å directly above Si atop sites.<sup>93,103</sup> However, the coverage of coherently scattering Br observed in these experiments was only found to be  $\leq 27\%$  of a monolayer, and the chemistry of the remaining portion of the surface was not identified.<sup>52–56</sup>

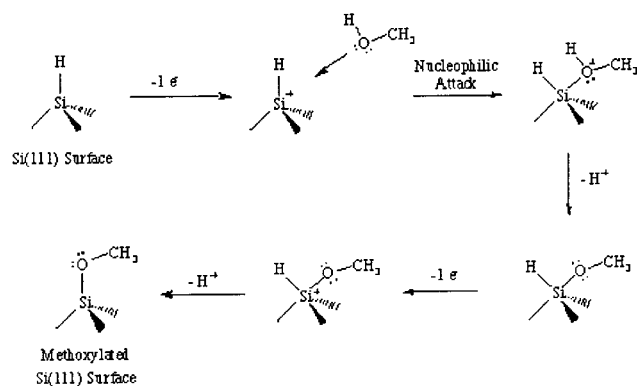
Our studies are consistent with the previous XSW data, but reveal an additional chemical transformation for these Si surfaces. The IR spectra clearly indicate the formation of surficial Si-OR bonds in such systems, as evidenced by the disappearance of Si-H stretches along with the formation of the diagnostic C-D stretch (for  $-\text{OCD}_3$  groups) at 2070 and 2225  $\text{cm}^{-1}$  (when deuterated alcohols are used as the alkoxy-

lating reagent). The comparable amplitudes of the  $\nu_s(\text{CD}_3)$  and  $\nu_{\text{as}}(\text{CD}_3)$  IR peaks observed for Si surfaces exposed to  $\text{Fc}^+$ ,  $\text{Br}_2$ , and  $\text{I}_2$  indicate that a significant portion of the surface sites have formed Si-OR bonds under these reaction conditions. The XPS data for the Si(111) surface do not show a clearly resolved oxidized Si peak at a position of  $\sim 100\text{--}101$  eV, which would be the expected peak position if an average oxidation state formula were used to estimate the Si 2p binding energy of a surficial Si- $\text{OCH}_3$  species. However, independent preparation of the alkoxyated surface from treatment of the chlorinated surface with neat alcohol indeed shows that the Si-O- $\text{CH}_3$  XPS peak on methoxylated Si surfaces is not well-separated from the bulk Si 2p peak. This observation is consistent with prior XPS studies, which have shown no peaks at high energies in the Si 2p region for Si surfaces exposed to  $\text{Fc}^+-\text{CH}_3\text{OH}$  solutions;<sup>81,94</sup> thus, at this instrumental resolution, XP spectra alone cannot generally provide diagnostic information on the formation of surficial Si alkoxide groups.

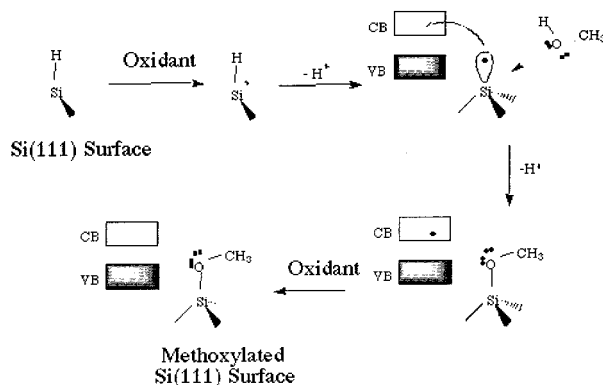
The relative XPS peak intensity ratios provide some indication of the coverage of the different species on the surfaces of interest. The variation in peak areas for the halogen-derived XPS signals relative to the Si 2p XPS signals was rather small over replicate samples, so the resulting peak intensity ratios are therefore considered to be quite reliable. The data clearly indicate that a significant coverage of halogens was present on surfaces that had been exposed to  $\text{I}_2-\text{CH}_3\text{OH}$  and  $\text{Br}_2-\text{CH}_3\text{OH}$  solutions, in addition to the Si- $\text{OCH}_3$  groups detected primarily by infrared spectroscopy. Converting XPS peak intensities into absolute surface coverages (expressed either as overlayer thicknesses or as fractional monolayers of the species of interest) requires the use of a structural model for the substrate and overlayer and requires estimation or experimental determination of several additional quantities such as escape depths. Given the well-documented sources and magnitudes of the errors involved in absolute coverage calculations,<sup>78</sup> the surface coverages derived herein for the halogen coverages are only considered accurate to within a factor of 2. Similarly, although the parameters involved in determining the coverage of oxidized Si are well-known for the instrument used in this work and although the coverage calculation involves estimation of fewer parameters because photoelectron cross sections are not needed when the methodology described herein is used to analyze the Si 2p region of the high-resolution XPS data, the relatively small absolute peak area of oxidized Si observed for the samples investigated in this work resulted again in overall relative coverage estimates that are only considered accurate to within a factor of 2. Additionally, the alkoxyated surfaces were relatively susceptible to oxidation, so the amounts of oxidized Si observed quoted in this work are upper limits to the actual amount of alkoxylation that results from contacting with the various solutions of interest in this study.

On a nonreconstructed Si(111) surface,  $-\text{OCH}_3$  groups cannot terminate every Si atop site because of the Si-Si atop distance being significantly smaller than the van der Waals diameter of a methoxyl group. Molecular modeling indicates that the maximum reasonable packing is obtained when every next-nearest-neighbor Si atop site is methoxylated, which would produce a 33% coverage of methoxylated surface atoms relative to the total number of Si(111) atop sites. The fractional coverages of oxidized Si observed in the high-resolution XPS scans of Si(111) surfaces exposed to  $\text{CH}_3\text{OH}-\text{Fc}^+$  solutions (Table 2) are thus consistent with values expected for an alkoxylation process. The wide-scan XPS data (Table 1) indicate additionally that surfaces exposed to methanolic solutions of

SCHEME 2



SCHEME 3

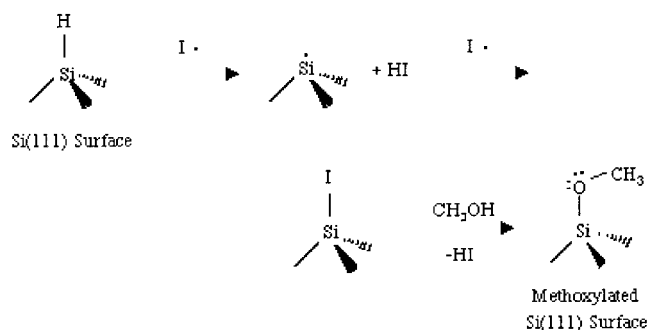


$\text{Br}_2$  or  $\text{I}_2$  possess significant silicon-halogen surface bonding. Given the errors in estimation of surface coverage by XPS, it is not appropriate to speculate on the precise structural features of such mixed-stoichiometry surfaces. However the XPS data are consistent with prior XSW data that have identified a relatively small fraction of the Si-X bonds as being located on atop sites on such surfaces. The (100)-oriented Si surfaces are less atomically smooth than the highly terraced surfaces that are obtained after  $\text{NH}_4\text{F}(\text{aq})$  treatment of (111)-oriented Si, so it is difficult to formulate a quantitative structural interpretation of the surfaces produced by exposure of HF-etched Si(100) surfaces to the oxidizing solutions studied in this work. For the (100)-oriented Si surface exposed to methanolic solutions of  $\text{Br}_2$  or  $\text{I}_2$ , the XPS data indicate even less coverage of silicon-halogen bonds than for the Si(111) surface, and the enhanced IR intensity of the C-D stretches observed on (100)-oriented Si suggests that the majority of the detectable species on this surface are Si-OR groups.

**C. Mechanisms for the Alkoxylation Reaction.** At least three possible mechanisms, depicted in Schemes 2–4, can be considered to account for the observed reactivity of the Si surface. In Scheme 2, the surficial Si-H is first oxidized by an electron acceptor to form a  $[\text{Si-H}]^+$  species. This  $[\text{Si-H}]^+$  species is then susceptible to nucleophilic attack by methanol, with subsequent loss of a proton, accompanied by another one-electron oxidation and proton loss, producing the final alkoxy-terminated Si surface. The five-coordinate Si intermediate has ample precedent in the chemistry of molecular Si species.<sup>104</sup>

An alternative pathway, which is analogous to that proposed for the electrochemical etching of Si in aqueous base<sup>94,96,105,106</sup> or in aqueous fluoride<sup>97,98,107,108</sup> solutions and which has been proposed to explain the anodic methoxylation of porous Si, is depicted in Scheme 3.<sup>77</sup> In this mechanism, following production of the  $[\text{Si-H}]^+$  species, the second electron in the Si-H bond

SCHEME 4



is transferred into the conduction band of Si during the nucleophilic attack rather than being immediately captured by a second equivalent of oxidant.

Scheme 4 depicts a radical-based reaction pathway in which  $\text{I}^\bullet$  abstracts a hydrogen atom from a Si-H bond, followed by subsequent attack of the surficial Si radical by a second  $\text{I}^\bullet$  to form a surficial Si-I group. This Si-I species can then either persist or react subsequently with alcohol to form HI and the alkoxy-terminated Si-OR species. This pathway provides an explanation for the formation of surficial Si-X ( $\text{X} = \text{I}, \text{Br}$ ) bonds during reaction of Si surfaces with alcoholic solutions of  $\text{I}_2$  or  $\text{Br}_2$  but obviously does not pertain to the Si surface reactivity that is observed during exposure to alcoholic ferrocenium solutions. It is also not clear how much, if any, of the surficial Si alkoxylation that is observed in alcoholic  $\text{I}_2$  or  $\text{Br}_2$  solutions proceeds through the formation of intermediate Si-X species, as opposed to being formed through the oxidative activation pathways (Schemes 2 or 3).

In the reaction pathways of either Scheme 2 or Scheme 3, the role of  $\text{I}_2$  to produce the initial activated  $[\text{Si-H}]^+$  species and to effect subsequent oxidation and alkoxylation could be served in principle by any other one-electron oxidant capable of oxidizing the surficial Si-H bonds, such as  $\text{Fc}^+$ . Electrochemical data indicate that the potential required to oxidize the surface bonds is approximately  $-0.3$  V vs SCE in the light (at n-type Si) and is  $\sim 0.1$  V vs SCE in the dark (at p-type Si).<sup>26,77</sup> Interestingly, a model compound,  $((\text{CH}_3)_3\text{Si})_3\text{SiH}$ , was inert toward nucleophilic attack in tetrahydrofuran in the presence of  $\text{Fc}^+$ , as monitored by  $^1\text{H}$  NMR spectrometry.  $((\text{CH}_3)_3\text{Si})_3\text{SiH}$  also did not display an anodic oxidation wave in  $\text{CH}_3\text{OH}-0.1$  M  $\text{LiClO}_4$  at potentials negative of those required to oxidize the solvent/electrolyte. To the extent that the localized molecular chemistry of the Si-H bonds on the (111)-oriented Si surface is well-modeled by the reactivity of the Si-H bond in  $((\text{CH}_3)_3\text{Si})_3\text{SiH}$ , the electrochemical data suggest that the one-electron oxidation product in the rate-determining step of the reaction (presumably the first oxidation process when anodic oxidation or one-electron outer-sphere oxidants or both are used) is stabilized by the presence of a band of orbitals in the crystalline Si solids under study. This would be consistent with either Scheme 2 or Scheme 3. To the extent that similar band-related stabilization occurs for other intermediates in the reaction pathway, the mechanism of Scheme 3 would be favored thermodynamically relative to the mechanism depicted in Scheme 2. The known ionization of HBr and HI in methanol provides precedent for the deprotonation of the  $[\text{Si-H}]^+$  species in Scheme 3 by the alcohol solvent. Furthermore, the energetics for this deprotonation process, combined with that for hole formation and localization at a Si surface atom in the presence of an oxidant, are likely more favorable than the energetics for H atom abstraction by  $\text{I}^\bullet$  radicals, suggesting that the mechanism

depicted in Scheme 3 may be favored in polar solvents relative to the mechanism depicted in Scheme 4 for energetic reasons.

It has also been proposed that alkoxylation of Si proceeds as part of a dissolution process.<sup>27</sup> However, previous work in our laboratory has shown that crystalline (100)-oriented Si surfaces in contact with either  $\text{CH}_3\text{OH}-\text{Fc}^{+/0}$  or  $\text{CH}_3\text{OH}-\text{Me}_2\text{Fc}^{+/0}$  electrolytes, which produce alkoxylation of Si surfaces (vide supra), exhibit a (negligible) average etching rate of  $\sim 6.6 \times 10^{-6} \text{ nm s}^{-1}$ .<sup>109</sup>

**D. Relationships between the Electronic and Chemical Properties of Alkoxylation of Si(111) Surfaces.** Si surfaces in contact with alcoholic  $\text{I}_2$  or  $\text{Br}_2$  solutions have been shown to display low effective surface recombination velocities under both low-level and high-level injection conditions.<sup>41–46</sup> This behavior has generally been ascribed to the passivating effects of Si–X bonding, producing an electrically active defect level of approximately 1 in  $10^5$  surface Si atoms.<sup>42–44</sup>

The present data clearly indicate that formation of Si–X bonding alone is not sufficient to provide a robust correlation between the electronic and chemical properties of such surfaces because Si surfaces in contact with  $\text{CH}_3\text{OH}-\text{Me}_2\text{Fc}^{+/0}$  electrolytes also display low effective surface recombination velocities after photoelectrochemical stabilization in  $\text{CH}_3\text{OH}-\text{Me}_2\text{Fc}^{+/0}$ .<sup>69</sup> As demonstrated above, such surfaces possess Si–OCH<sub>3</sub> bonds, and no Si–X (X = Br, I) bonds are formed under such conditions. The observation that n-Si photoanodes in contact with acetone–75 mM ferrocenium<sup>+/0</sup> solutions are dominated by surface recombination processes<sup>110</sup> whereas n-Si/CH<sub>3</sub>OH–Me<sub>2</sub>Fc<sup>+/0</sup> or n-Si/propylene carbonate–methanol–Me<sub>2</sub>Fc<sup>+/0</sup> contacts exhibit bulk recombination-limited junction behavior<sup>69,70</sup> is also consistent with the hypothesis that alkoxylation produces a surface having superior electronic properties to the surface obtained from immersion of H-terminated Si into such electrolytes. A reasonable hypothesis is therefore that alkoxylation, as opposed to Si–X (X = Br, I) bond formation, is correlated with low recombination velocities of such Si surfaces.

The situation in contact with these redox-active electrolytes is complicated, however, by the presence of band bending of the Si due to electrochemical exchange reactions between charge carriers in the Si and the redox-active species in the electrolyte. Recent work has in fact shown that electrochemical charge transfer and concomitant formation of a carrier inversion layer at the Si surface are predominantly responsible for producing the low effective surface recombination velocities for n-Si surfaces in contact with electrolytes having electrochemical potentials close to the Si valence band energy.<sup>111</sup> This is the case for n-Si exposed to methanolic solutions containing  $\text{Fc}^+$ ,  $\text{I}_2$ , and  $\text{Br}_2$ , so the effects of electrical trap levels in such systems are largely screened by inversion layer formation, which, in turn, produces a low effective surface recombination velocity over a wide range of values of the actual surface electrical trap density.

Measurements of the surface recombination velocity in contact with a  $\text{N}_2(\text{g})$  ambient eliminate the effect of inversion layer formation and reveal significant differences in surface recombination velocity between Si samples that have been exposed to  $\text{CH}_3\text{OH}-\text{Fc}^+$  or  $\text{CH}_3\text{OH}-\text{I}_2$  solutions.<sup>111</sup> Such studies have shown that exposure to  $\text{CH}_3\text{OH}-\text{Fc}^+$  electrolytes produces a surface having an initial recombination velocity in  $\text{N}_2(\text{g})$  of  $70 \text{ cm s}^{-1}$ , whereas surfaces exposed to  $\text{CH}_3\text{OH}-\text{I}_2$  have a much higher  $S$  value ( $810 \text{ cm s}^{-1}$ ). The mixed-stoichiometry surface obtained from exposure of (111)-oriented Si to  $\text{CH}_3\text{OH}-\text{I}_2$  therefore has a relatively high surface electrical defect density and is not suitable for use in many electronic device applications. In contrast, the alkoxylation of Si(111) surface

obtained from immersion into the one-electron oxidant  $\text{Fc}^+$  has a much lower  $S$  value, consistent with the more homogeneous surface chemistry produced by this procedure. The air stability of the alkoxylation of Si surface, however, is inferior to that of the alkylated Si surface<sup>112</sup> and in fact is inferior to the H-terminated Si(111) surface,<sup>112</sup> so alkylation, and specifically methylation, is preferred with respect to alkoxylation to obtain air stable, electronically superior Si surfaces. Additionally, the lack of efficient packing of alkoxy groups on the Si(111) surface produces higher initial surface recombination velocities and inferior surface stabilities to oxidation than are available from methylated Si surfaces.<sup>111,113</sup> Thus, alkoxylation of Si surfaces are useful for controlling the initial electronic behavior of such surfaces, but further approaches to chemical stabilization will be required to effect long-term stability in air from such alkoxylation of Si systems.

## V. Conclusions

H-terminated Si(111) and Si(100) surfaces react to form Si–OR groups upon exposure to alcohol solutions containing the oxidizing agents  $\text{Fc}^+$ ,  $\text{I}_2$ , or  $\text{Br}_2$ . Under our reaction conditions, no detectable reaction occurred upon immersion of the H-terminated surfaces into anhydrous, oxygen-free alcohols or upon immersion into alcoholic solutions that contained non-oxidizing species such as ferrocene. A mixed-stoichiometry surface is produced by immersion of H-terminated Si surfaces into alcoholic solutions that contain  $\text{I}_2$  or  $\text{Br}_2$ , consistent with prior X-ray standing wave measurements and other data on Si surfaces exposed to alcoholic solutions of  $\text{Br}_2$ . Formation of Si–X (X = Br, I) bonding alone is not sufficient to provide a robust correlation between the electronic and chemical properties of such crystalline Si surfaces, whereas formation of silicon–alkoxy bonds appears to be a common motif for surfaces often used in electronic and electrochemical studies of Si.

**Acknowledgment.** We acknowledge the NSF, Grant CHE-9974562, for support of this work.

**Supporting Information Available:** FT-IR spectra of Si-(111) surfaces after immersion in  $\text{NH}_4\text{F}(\text{aq})$ ,  $\text{CH}_3\text{OH}$ ,  $\text{CH}_3\text{OH}-\text{Fc}$ ,  $\text{CH}_3\text{OH}-\text{FcBF}_4$ ,  $\text{CH}_3\text{OH}-\text{I}_2$ ,  $\text{CH}_3\text{OH}-\text{Br}_2$ ,  $\text{C}_4\text{H}_9\text{OH}$ ,  $\text{C}_4\text{H}_9\text{OH}-\text{Fc}$ , and  $\text{C}_4\text{H}_9\text{OH}-\text{FcBF}_4$ ; FT-IR spectra of Si(111) after chlorination with  $\text{C}_6\text{H}_5\text{Cl}-\text{PCl}_5$ , followed by reaction with  $\text{CH}_3\text{OH}-\text{LiOCH}_3$ ; survey and high-resolution XP spectra of Si(111) surfaces immersed into  $\text{NH}_4\text{F}(\text{aq})$ ,  $\text{HO}(\text{CH}_2)_3\text{CF}_3$ ,  $\text{HO}(\text{CH}_2)_3\text{CF}_3-\text{Fc}$ , and  $\text{HO}(\text{CH}_2)_3\text{CF}_3-\text{FcBF}_4$ ; survey and high-resolution XP spectra of Si(111) after  $\text{NH}_4\text{F}(\text{aq})$  etching, chlorination with  $\text{C}_6\text{H}_5\text{Cl}-\text{PCl}_5$ , and following reaction of the chlorinated surface with  $\text{CD}_3\text{OD}-\text{LiOCD}_3$  or  $\text{THF}-\text{LiO}(\text{CH}_2)_3\text{CF}_3$ ; FT-IR spectra of Si(100) surfaces after immersion in 48%  $\text{HF}(\text{aq})$ ,  $\text{CH}_3\text{OH}$ ,  $\text{CH}_3\text{OH}-\text{Fc}$ ,  $\text{CH}_3\text{OH}-\text{FcBF}_4$ ,  $\text{CH}_3\text{OH}-\text{I}_2$ , and  $\text{CH}_3\text{OH}-\text{Br}_2$ ; survey XP spectra of Si(100) surfaces after immersion in 48%  $\text{HF}(\text{aq})$ ,  $\text{CD}_3\text{OD}-\text{FcBF}_4$ ,  $\text{CD}_3\text{OD}-\text{I}_2$ , and  $\text{CD}_3\text{OD}-\text{Br}_2$ ; FT-IR spectra of Si(100) after chlorination with  $\text{C}_6\text{H}_5\text{Cl}-\text{PCl}_5$ , followed by reaction with  $\text{CH}_3\text{OH}-\text{LiOCH}_3$ ; survey and high-resolution XP spectra of Si(100) after 48%  $\text{HF}(\text{aq})$  etching, chlorination with  $\text{C}_6\text{H}_5\text{Cl}-\text{PCl}_5$ , and following reaction of the chlorinated surface with  $\text{CD}_3\text{OD}-\text{LiOCD}_3$ . This material is available free of charge via the Internet at <http://pubs.acs.org>.

## References and Notes

- (1) Bansal, A.; Li, X. L.; Lauermann, I.; Lewis, N. S.; Yi, S. I.; Weinberg, W. H. *J. Am. Chem. Soc.* **1996**, *118*, 7225–7226.

- (2) Terry, J.; Mo, R.; Wigren, C.; Cao, R. Y.; Mount, G.; Pianetta, P.; Linford, M. R.; Chidsey, C. E. D. *Nucl. Instrum. Methods Phys. Res., Sect. B* **1997**, *133*, 94–101.
- (3) Terry, J.; Linford, M. R.; Wigren, C.; Cao, R. Y.; Pianetta, P.; Chidsey, C. E. D. *Appl. Phys. Lett.* **1997**, *71*, 1056–1058.
- (4) Terry, J.; Linford, M. R.; Wigren, C.; Cao, R. Y.; Pianetta, P.; Chidsey, C. E. D. *J. Appl. Phys.* **1999**, *85*, 213–221.
- (5) He, J.; Patitsas, S. N.; Preston, K. F.; Wolkow, R. A.; Wayner, D. D. M. *Chem. Phys. Lett.* **1998**, *286*, 508–514.
- (6) Boukherroub, R.; Morin, S.; Bensebaa, F.; Wayner, D. D. M. *Langmuir* **1999**, *15*, 3831–3835.
- (7) Boukherroub, R.; Wayner, D. D. M. *J. Am. Chem. Soc.* **1999**, *121*, 11513–11515.
- (8) Effenberger, F.; Gotz, G.; Bidlingmaier, B.; Wezstein, M. *Angew. Chem., Int. Ed.* **1998**, *37*, 2462–2464.
- (9) Cicero, R. L.; Linford, M. R.; Chidsey, C. E. D. *Langmuir* **2000**, *16*, 5688–5695.
- (10) Linford, M. R.; Chidsey, C. E. D. *J. Am. Chem. Soc.* **1993**, *115*, 12631–12632.
- (11) Linford, M. R.; Fenter, P.; Eisenberger, P. M.; Chidsey, C. E. D. *J. Am. Chem. Soc.* **1995**, *117*, 3145–3155.
- (12) Sieval, A. B.; Demirel, A. L.; Nissink, J. W. M.; Linford, M. R.; van der Maas, J. H.; de Jeu, W. H.; Zuilhof, H.; Sudholter, E. J. R. *Langmuir* **1998**, *14*, 1759–1768.
- (13) Sung, M. M.; Kluth, G. J.; Yauw, O. W.; Maboudian, R. *Langmuir* **1997**, *13*, 6164–6168.
- (14) Zazzera, L. A.; Evans, J. F.; Deruelle, M.; Tirrell, M.; Kessel, C. R.; McKeown, P. J. *Electrochem. Soc.* **1997**, *144*, 2184–2189.
- (15) Yu, H. Z.; Boukherroub, R.; Morin, S.; Wayner, D. D. M. *Electrochem. Commun.* **2000**, *2*, 562–566.
- (16) Mitchell, S. A.; Boukherroub, R.; Anderson, S. J. *Phys. Chem. B* **2000**, *104*, 7668–7676.
- (17) Fidelis, A.; Ozanam, F.; Chazalviel, J. N. *Surf. Sci.* **2000**, *444*, L7–L10.
- (18) Gros-Jean, M.; Herino, R.; Chazalviel, J. N.; Ozanam, F.; Lincot, D. *Mater. Sci. Eng., B* **2000**, *69*, 77–80.
- (19) Allongue, P.; de Villeneuve, C. H.; Pinson, J.; Ozanam, F.; Chazalviel, J. N.; Wallart, X. *Electrochim. Acta* **1998**, *43*, 2791–2798.
- (20) Allongue, P.; de Villeneuve, C. H.; Pinson, J. *Electrochim. Acta* **2000**, *45*, 3241–3248.
- (21) Bergerson, W. F.; Mulder, J. A.; Hsung, R. P.; Zhu, X. Y. *J. Am. Chem. Soc.* **1999**, *121*, 454–455.
- (22) Zhu, X. Y.; Mulder, J. A.; Bergerson, W. F. *Langmuir* **1999**, *15*, 8147–8154.
- (23) Zhu, X. Y.; Boiadjev, V.; Mulder, J. A.; Hsung, R. P.; Major, R. C. *Langmuir* **2000**, *16*, 6766–6772.
- (24) Lee, E. J.; Bitner, T. W.; Ha, J. S.; Shane, M. J.; Sailor, M. J. *J. Am. Chem. Soc.* **1996**, *118*, 5375–5382.
- (25) Boukherroub, R.; Morin, S.; Sharpe, P.; Wayner, D. D. M.; Allongue, P. *Langmuir* **2000**, *16*, 7429–7434.
- (26) Haber, J. A.; Lauerma, I.; Michalak, D.; Vaid, T. P.; Lewis, N. S. *J. Phys. Chem. B* **2000**, *104*, 9947–9950.
- (27) Kim, N. Y.; Laibinis, P. E. *J. Am. Chem. Soc.* **1997**, *119*, 2297–2298.
- (28) Cleland, G.; Horrocks, B. R.; Houlton, A. J. *Chem. Soc. Faraday Trans.* **1995**, *91*, 4001–4003.
- (29) Eagling, R. D.; Bateman, J. E.; Goodwin, N. J.; Henderson, W.; Horrocks, B. R.; Houlton, A. J. *Chem. Soc. Dalton Trans.* **1998**, 1273–1275.
- (30) Bateman, J. E.; Eagling, R. D.; Horrocks, B. R.; Houlton, A. J. *Phys. Chem. B* **2000**, *104*, 5557–5565.
- (31) Sailor, M. J.; Lee, E. J. *Adv. Mater.* **1997**, *9*, 783.
- (32) Song, J. H.; Sailor, M. J. *Comments Inorg. Chem.* **1999**, *21*, 69–84.
- (33) Buriak, J. M. *Chem. Commun.* **1999**, 1051–1060.
- (34) Buriak, J. M. *Adv. Mater.* **1999**, *11*, 265–267.
- (35) Wolkow, R. A. *Annu. Rev. Phys. Chem.* **1999**, *50*, 413–441.
- (36) Teplyakov, A. V.; Kong, M. J.; Bent, S. F. *J. Am. Chem. Soc.* **1997**, *119*, 11100–11101.
- (37) Hamers, R. J.; Coulter, S. K.; Ellison, M. D.; Hovis, J. S.; Padowitz, D. F.; Schwartz, M. P.; Greenlief, C. M.; Russell, J. N. *Acc. Chem. Res.* **2000**, *33*, 617–624.
- (38) Lopinski, G. P.; Wayner, D. D. M.; Wolkow, R. A. *Nature* **2000**, *406*, 48–51.
- (39) Bansal, A.; Lewis, N. S. *J. Phys. Chem. B* **1998**, *102*, 1067–1070.
- (40) Bansal, A.; Lewis, N. S. *J. Phys. Chem. B* **1998**, *102*, 4058–4060.
- (41) Reddy, A. J.; Chan, J. V.; Burr, T. A.; Mo, R.; Wade, C. P.; Chidsey, C. E. D.; Michel, J.; Kimerling, L. C. *Physica B* **1999**, *274*, 468–472.
- (42) Reddy, A. J.; Burr, T. A.; Chan, J. K.; Norga, G. J.; Michel, J.; Kimerling, L. C. Silicon surface defects: The roles of passivation and surface contamination. In *Defects in Semiconductors, ICDS-19*; Davies, G.; Nazaré, M. H., Eds.; Trans Tech Publications: Uetikon-Zuerich, Switzerland, 1997; Vol. 258-2, Parts 1–3, pp 1719–1724.
- (43) Horanyi, T. S.; Pavelka, T.; Tutto, P. *Appl. Surf. Sci.* **1993**, *63*, 306–311.
- (44) Msaad, H.; Michel, J.; Lappe, J. J.; Kimerling, L. C. *J. Electron. Mater.* **1994**, *23*, 487–491.
- (45) Stephens, A. W.; Green, M. A. *Sol. Energy Mater. Sol. Cells* **1997**, *45*, 255–265.
- (46) Kurita, K.; Shingouji, T. *Jpn. J. Appl. Phys.* **1999**, *38*, 5710–5714.
- (47) Larkins, G. L.; Fung, C. D.; Rickert, S. E. *Thin Solid Films* **1989**, *180*, 217–225.
- (48) Chabal, Y. J.; Harris, A. L.; Raghavachari, K.; Tully, J. C. *Int. J. Mod. Phys. B* **1993**, *7*, 1031–1078.
- (49) Jakob, P.; Chabal, Y. J.; Raghavachari, K.; Dumas, P.; Christman, S. B. *Surf. Sci.* **1993**, *285*, 251–258.
- (50) Higashi, G. S.; Chabal, Y. J.; Trucks, G. W.; Raghavachari, K. *Appl. Phys. Lett.* **1990**, *56*, 656–658.
- (51) Wade, C. P.; Chidsey, C. E. D. *Appl. Phys. Lett.* **1997**, *71*, 1679–1681.
- (52) Cowan, P. L.; Golovchenko, J. A.; Robbing, M. F. *Phys. Rev. Lett.* **1980**, *44*, 1680–1683.
- (53) Golovchenko, J. A.; Patel, J. R.; Kaplan, D. R.; Cowan, P. L.; Bedzyk, M. J. *Phys. Rev. Lett.* **1982**, *49*, 560–563.
- (54) Materlik, G.; Frahm, A.; Bedzyk, M. J. *Phys. Rev. Lett.* **1984**, *52*, 441–444.
- (55) Bedzyk, M. J.; Gibson, W. M.; Golovchenko, J. A. *J. Vac. Sci. Technol.* **1982**, *20*, 634–637.
- (56) Dev, B. N.; Aristov, V.; Hertel, N.; Thundat, T.; Gibson, W. M. *Surf. Sci.* **1985**, *163*, 457–477.
- (57) Funke, P.; Materlik, G. *Solid State Commun.* **1985**, *54*, 921–923.
- (58) Funke, P.; Materlik, G. *Surf. Sci.* **1987**, *188*, 378–390.
- (59) Michel, E. G.; Pauly, T.; Eteläniemi, V.; Materlik, G. *Surf. Sci.* **1991**, *241*, 111–123.
- (60) Stephens, A. W.; Green, M. A. *J. Appl. Phys.* **1996**, *80*, 3897–3903.
- (61) Sekar, K.; Satyam, P. V.; Kuri, G.; Mahapatra, D. P.; Dev, B. N. *Nucl. Instrum. Methods Phys. Res., Sect. B* **1992**, *71*, 308–313.
- (62) Sekar, K.; Satyam, P. V.; Kuri, G.; Mahapatra, D. P.; Dev, B. N. *Nucl. Instrum. Methods Phys. Res., Sect. B* **1993**, *73*, 63–70.
- (63) Sekar, K.; Kuri, G.; Satyam, P. V.; Sundaravel, B.; Mahapatra, D. P.; Dev, B. N. *Solid State Commun.* **1995**, *96*, 871–875.
- (64) Sekar, K.; Kuri, G.; Satyam, P. V.; Sundaravel, B.; Mahapatra, D. P.; Dev, B. N. *Surf. Sci.* **1995**, *339*, 96–104.
- (65) Sekar, K.; Kuri, G.; Satyam, P. V.; Sundaravel, B.; Mahapatra, D. P.; Dev, B. N. *Phys. Rev. B: Condens. Matter Mater. Phys.* **1995**, *51*, 14330–14336.
- (66) Sundaravel, B.; Das, A. K.; Ghose, S. K.; Sekar, K.; Dev, B. N. *Appl. Surf. Sci.* **1999**, *137*, 11–19.
- (67) Sekar, K.; Sundaravel, B.; Wilson, I. H.; Heiland, W. *Appl. Surf. Sci.* **2000**, *156*, 161–168.
- (68) Rout, B.; Sundaravel, B.; Das, A. K.; Ghose, S. K.; Sekar, K.; Mahapatra, D. P.; Dev, B. N. *J. Vac. Sci. Technol., B* **2000**, *18*, 1847–1852.
- (69) Rosenbluth, M. L.; Lewis, N. S. *J. Am. Chem. Soc.* **1986**, *108*, 4689–4695.
- (70) Gibbons, J. F.; Cogan, G. W.; Gronet, C. M.; Lewis, N. S. *Appl. Phys. Lett.* **1984**, *45*, 1095–1097.
- (71) Lewis, N. S. *Acc. Chem. Res.* **1990**, *23*, 176–183.
- (72) Tan, M. X.; Laibinis, P. E.; Nguyen, S. T.; Kesselman, J. M.; Stanton, C. E.; Lewis, N. S. *Prog. Inorg. Chem.* **1994**, *41*, 21–144.
- (73) Rosenbluth, M. L.; Lewis, N. S. *J. Electrochem. Soc.* **1987**, *134*, C463–C464.
- (74) Rosenbluth, M. L.; Lewis, N. S. *J. Phys. Chem.* **1989**, *93*, 3735–3740.
- (75) Fajardo, A. M.; Lewis, N. S. *J. Phys. Chem. B* **1997**, *101*, 11136–11151.
- (76) Chazalviel, J. N. *J. Electroanal. Chem.* **1987**, *233*, 37–48.
- (77) Warntjes, M.; Vieillard, C.; Ozanam, F.; Chazalviel, J. N. *J. Electrochem. Soc.* **1995**, *142*, 4138–4142.
- (78) Briggs, D.; Seah, M. P. *Practical Surface Analysis: Auger and X-ray Photoelectron Spectroscopy*, 2nd ed.; Wiley: New York, 1990; Vol. 1.
- (79) Scofield, J. H. *J. Electron Spectrosc. Relat. Phenom.* **1976**, *8*, 129.
- (80) Oxtoby, D. W.; Nachtrieb, N. H.; Freeman, W. A. *Chemistry, Science of Change*, 2nd ed.; Saunders College Publishing: Philadelphia, PA, 1994.
- (81) Tufts, B. J.; Kumar, A.; Bansal, A.; Lewis, N. S. *J. Phys. Chem.* **1992**, *96*, 4581–4592.
- (82) Laibinis, P. E.; Bain, C. D.; Whitesides, G. M. *J. Phys. Chem.* **1991**, *95*, 7017–7021.
- (83) Pomykal, K. E.; Fajardo, A. M.; Lewis, N. S. *J. Phys. Chem.* **1995**, *99*, 8302–8310.
- (84) Hochella, M. F.; Carim, A. H. *Surf. Sci.* **1988**, *197*, L260–L268.
- (85) McFeely, F. R.; Morar, J. F.; Shinn, N. D.; Landgren, G.; Himpel, F. J. *Phys. Rev. B* **1984**, *30*, 764–770.

- (86) Himpsel, F. J.; McFeely, F. R.; Talebibrabimi, A.; Yarmoff, J. A.; Hollinger, G. *Phys. Rev. B* **1988**, *38*, 6084–6096.
- (87) Chakarian, V.; Shuh, D. K.; Yarmoff, J. A.; Hakansson, M. C.; Karlsson, U. O. *Surf. Sci.* **1993**, *296*, 383–392.
- (88) Hill, J. M.; Royce, D. G.; Fadley, C. S.; Wagner, L. F.; Grunthaner, F. J. *Chem. Phys. Lett.* **1976**, *44*, 225–231.
- (89) Fadley, F. S. *Prog. Solid State Chem.* **1976**, *11*, 265–343.
- (90) Lifshits, V. G.; Saranin, A. A.; Zotov, A. V. *Surface Phases on Silicon*; John Wiley and Sons: New York, 1994.
- (91) Sieval, A. B.; van den Hout, B.; Zuilhof, H.; Sudholter, E. J. R. *Langmuir* **2000**, *16*, 2987–2990.
- (92) Fajardo, A. M.; Lewis, N. S. *Science* **1996**, *274*, 969–972.
- (93) Lewis, N. S. *J. Phys. Chem. B* **1998**, *102*, 4843–4855.
- (94) Shimanouchi, T. *Tables of Molecular Vibrational Frequencies Consolidated Volume I*; National Bureau of Standards: Washington, DC, 1972; Vol. I.
- (95) No Fe signal was detectable on this surface; thus, the F likely originated from the  $\text{BF}_4^-$  species. Boron could not be detected by XPS because its cross section is small (0.486 vs 3.40 for F) and because its peak position is superimposed on the 2nd bulk plasmon resonance of the Si 2s peak.
- (96) Ye, S.; Ichihara, T.; Uosaki, K. *Appl. Phys. Lett.* **1999**, *75*, 1562–1564.
- (97) Green, W. H.; Lee, E. J.; Lauerhaas, J. M.; Bitner, T. W.; Sailor, M. J. *Appl. Phys. Lett.* **1995**, *67*, 1468–1470.
- (98) Chabal, Y. J.; Higashi, G. S.; Raghavachari, K.; Burrows, V. A. *J. Vac. Sci. Technol., A* **1989**, *7*, 2104–2109.
- (99) Robins, E. G.; Stewart, M. P.; Buriak, J. M. *Chem. Commun.* **1999**, 2479–2480.
- (100) Stewart, M. P.; Buriak, J. M. *Angew. Chem., Int. Ed.* **1998**, *37*, 3257–3260.
- (101) Bateman, J. E.; Horrocks, B. R.; Houlton, A. *J. Chem. Soc. Faraday Trans.* **1997**, *93*, 2427–2431.
- (102) Henderson, R. C.; Polito, W. J. *Surf. Sci.* **1969**, *14*, 473–477.
- (103) Cheng, H. S.; Luo, L.; Okamoto, M.; Thundat, T.; Hashimoto, S.; Gibson, W. M. *J. Vac. Sci. Technol., A* **1987**, *5*, 607–610.
- (104) Greenwood, N. N.; Earnshaw, A. *Chemistry of the Elements*; Pergamon: New York, 1984.
- (105) Allongue, P.; Costa-Kieling, V.; Gerischer, H. *J. Electrochem. Soc.* **1993**, *140*, 1009–1018.
- (106) Allongue, P.; Costa-Kieling, V.; Gerischer, H. *J. Electrochem. Soc.* **1993**, *140*, 1018–1026.
- (107) Gerischer, H.; Allongue, P.; Costa-Kieling, V. *Ber. Bunsen-Ges. Phys. Chem.* **1993**, *97*, 753–756.
- (108) Allongue, P.; Kieling, V.; Gerischer, H. *Electrochim. Acta* **1995**, *40*, 1353–1360.
- (109) Shreve, G. A.; Karp, C. D.; Pomykal, K. E.; Lewis, N. S. *J. Phys. Chem.* **1995**, *99*, 5575–5580.
- (110) Mao, D.; Kim, K. J.; Frank, A. J. *J. Electrochem. Soc.* **1994**, *141*, 1231–1236.
- (111) Royea, W. J.; Michalak, D. J.; Lewis, N. S. *Appl. Phys. Lett.* **2000**, *77*, 2566–2568.
- (112) Haber, J. A.; Michalak, D.; Lewis, N. S., to be submitted for publication.
- (113) Royea, W. J.; Juang, A.; Lewis, N. S. *Appl. Phys. Lett.* **2000**, *77*, 1988–1990.